Propagation of extragalactic high energy cosmic and γ rays

Sangjin Lee

Department of Physics, Enrico Fermi Institute, The University of Chicago, Chicago, Illinois 60637-1433
and NASA/Fermilab Astrophysics Center, Fermi National Accelerator Laboratory, Batavia, Illinois 60510-0500

The observation of air showers from elementary particles with energies exceeding 10^{20} eV poses a puzzle to the physics and astrophysics of cosmic rays which is still unresolved. Explaining the origin and nature of these particles is a challenge. In order to constrain production mechanisms and sites, one has to account for the processing of particle spectra by interactions with radiation backgrounds and magnetic fields on the way to the observer. In this paper, I report on an extensive study on the propagation of extragalactic nucleons, γ-rays, and electrons in the energy range between 10^8 eV and 10^{25} eV. We have devised an efficient numerical method to solve the transport equations for cosmic ray spectral evolution. The universal radiation background spectrum in the energy range between $\simeq 10^{-9}$ eV and $\simeq 10$ eV is considered in the numerical code, including the diffuse radio background, the cosmic microwave background, and the infrared-optical background, as well as a possible extragalactic magnetic field. We apply the code to compute the particle spectra predicted by several models of ultrahigh energy cosmic ray origin. A comparison with the observed fluxes, especially the diffuse γ-ray background in several energy ranges, allows one to constrain certain classes of models. [S0556-2821(98)07916-8]

PACS number(s): 98.70.Sa, 98.70.Rz, 98.80.Cq

I. INTRODUCTION

Shortly after the cosmic microwave background (CMB) was discovered [1] it became clear that this universal radiation field has profound implications for the astrophysics of ultrahigh energy cosmic rays (UHE CR) of energies above 10^{18} eV. For nucleons the most profound effect is photoproduction of pions on the CMB. Known as the Greisen-Zatsepin-Kuz'min (GZK) ''cutoff'' [2,3], this effect leads to a steep drop in their energy attenuation length by about a factor of 100 at around 6×10^{19} eV which corresponds to the threshold for this process. The nucleon attenuation length above this threshold is about 10 Mpc. Heavy nuclei with energies above about 10^{19} eV are photodisintegrated in the field of the CMB within a few Mpc [4]. One of the major unresolved questions in cosmic ray physics is the existence or non-existence of a cutoff in the UHE CR spectrum at a few 10^{19} eV which, in the case of extragalactic sources, could be attributed to these effects.

Therefore, there has been renewed interest in UHE CR research since events with energies exceeding 10^{20} eV have been detected. The Haverah Park experiment [7] reported several events with energies near or slightly above 10^{20} eV. The Fly's Eye experiment [8,9] detected the world's highest energy CR event to date, with an energy $\simeq 3 \times 10^{20}$ eV. Near the arrival direction of this event the Yakutsk experiment [10] was recorded another event of energy $\simeq 1.1 \times 10^{20}$ eV. More recently, the Akeno Giant Air Shower Array (AGASA) experiment [11,12] has also reported an event with energy $1.7 - 2.6 \times 10^{20}$ eV. At present, It is unclear whether these events indicate a spectrum continuing beyond 10^{20} eV without any cutoff or the existence of a cutoff followed by a recovery in the form of a ''gap'' in the spectrum [13].

There has been much speculation about the nature and origin of these highest energy cosmic rays (HECRs) [14–18]. Concerning the production mechanism one can dis-tinguish between two broad classes of models: Within acceleration models, charged primaries, namely protons and heavy nuclei are accelerated to very high energies [19,20] in a ''bottom-up'' manner. Preferred sites are large-scale astrophysical shocks which occur for instance in radio galaxies [21]. Even in these objects it seems hardly possible to accelerate CRs to the required energies [14,22,23]. Recently it has also been suggested that acceleration of UHE CRs could be associated with cosmological gamma-ray bursts (GRBs) [24–26]. In the second class of so called ''top-down'' models, charged and neutral primaries are produced at UHEs in the first place, typically by quantum mechanical decay of supermassive elementary X particles related to grand unified theories (GUTs). Sources of such particles at present could be topological defects (TDs) left over from early universe phase transitions caused by the spontaneous breaking of symmetries underlying these GUTs [27–34]. The injection spectra in top-down models tend to be considerably harder (flatter) than in acceleration models.

The issue of the particle identity of the UHE CRs is not resolved completely yet. The Fly's Eye analysis [8] suggested a transition from a spectrum dominated by heavy nuclei to a predominantly light composition above a few times 10^{19} eV. However, this has not been confirmed by the AGASA experiment [36]. On the other hand, γ-rays as the UHE CRs had been usually disfavored on two grounds. First, the shower profile of the highest energy Fly's Eye event indicates that it may be inconsistent with a γ-ray primary [37]. Also, some models that implies γ-ray primaries often predict UHE CR fluxes that are too small to be detected [38]. However, neither arguments are definitive yet, because the shower development in the atmosphere depends sensitively on parameters that are rather uncertain such as the strength and the orientation of the geomagnetic field. There is also a suggestion that the Fly's Eye shower profile may be incon-

sistent even with a proton primary [39].

Other options discussed for the nature of the HECRs include heavy nuclei and even neutrinos [37]. Heavy nuclei have their own merits because they can be deflected considerably by the galactic magnetic field which relaxes the source direction requirements [8,11]. In addition, for shock acceleration, heavy nuclei can be accelerated to higher terminal energies because of their larger charge. However, one should note that the range for heavy nuclei is limited to a few Mpc as mentioned above. Neutrinos, on the other hand, do not lose much energy over cosmological distances [40,41], but by the same token the probability for interacting in the atmosphere is small. Attributing the HECRs to neutrinos would therefore require a neutrino flux at UHEs which is much higher than the observed CR flux at the same energies. This poses severe constraints on the possible sources for these neutrinos [42]. In addition, neutrinos would give rise to predominantly deeply penetrating showers in the atmosphere.

The initially produced spectrum of UHE CRs is modified during their propagation. There are many studies on nucleon propagation in the literature using analytical [43–46] as well as numerical approaches [17,47–49], and the propagation of heavy nuclei has also been considered [17]. This was mainly motivated by the conventional acceleration models which usually predict UHE CR fluxes to be dominated by these particles. However, secondary γ-rays and neutrinos can also be produced, for example as decay products of pions created by interactions with various radiation backgrounds at the source or during propagation [48]. Under certain circumstances their flux can become comparable with the primary flux [50]. Furthermore, within TD models γ-rays are expected to dominate to begin with [51]. A study on γ-ray propagation in this context has been performed recently [52,53] using a quantitative treatment on the cascade initiated by UHE photons. In my opinion, however, it suffers from several unrealistic assumptions with respect to the injection scenarios considered. We improve on their treatment of the propagation of γ-rays. Apart from that, we find three reasons to explore UHE γ-ray propagation in more detail in this paper:

First, due to the absence of threshold effects similar to photopion production which causes the GZK ''cutoff'' for nucleons, the γ-ray spectrum is not expected to have a break around 10^{20} eV. Furthermore, γ-rays can generate electromagnetic (EM) cascades while propagating rather than being absorbed right away. UHE electrons produced by pair production upscatter background photons and transfer most of the energy back to photons. This effect considerably increases the effective energy attenuation length of the ''cascade'' photons [54,55]. At a few times 10^{20} eV this attenuation length may be even greater than that for protons which drops precipitously at the threshold for photopion production. Extragalactic γ-rays could therefore have some potential to produce a recovery beyond the GZK ''cutoff.''

Second, in contrast to the case of nucleons, the propagation of γ-rays is presently fraught by certain ambiguities which are mainly due to uncertainties in the intensity of the universal radio background and the strength and spectrum of the extragalactic magnetic field (EGMF). We hope that an application of the general framework presented here under different assumptions for such parameters could in turn provide some insights into their actual values once the UHE γ-ray flux is known to some accuracy. This would be in analogy to the method of using TeV γ-ray observations to constrain or detect the universal infrared-optical background [56]. In previous work [54] it is shown that, depending on its strength, the large-scale EGMF could produce a feature in the γ-ray spectrum which might be observable in the future.

Finally, the study of high energy cosmic and γ-ray propagation can place stringent constraints on the nature and origin of UHE CRs. Such constraints can be obtained by computing the propagation modified spectra especially of lower energy γ-rays expected within a certain scenario and comparing the predictions with the observed fluxes [50,57,58]. At UHEs there are some experimental prospects to distinguish γ-rays from other primaries in the future, possibly even on an event by event basis [59]. This would allow comparing not only the total fluxes of UHE nucleons, heavy nuclei, and γ-rays, but also their composition with model predictions.

This motivated the present comprehensive study of propagation of γ-rays and nucleons and its application to models which attribute UHE CRs to top-down mechanisms within GUT-scale physics or associate them with cosmological gamma ray bursts (GRBs). We explore the energy range of $10^8 < E < 10^{25}$ eV. The low end is chosen such that we can draw constraints by comparing the propagated spectra with existing measurements of the diffuse γ-ray background around 100 MeV [60–62]. The high end is chosen beyond the highest CR energies ever observed and reaches the typical GUT scale energy, enabling us to study top-down models. We include not only the CMB but also the diffuse radio background which plays a big role at the highest energies and the infrared-optical (IR-O) background which influences the flux at somewhat lower energies. We also include the EGMF as a free parameter. The propagation of nucleons is also studied with special emphasis on the production of secondary γ-rays, electrons, and neutrinos.

The rest of the paper is organized as follows: In Sec. II, we present the general ingredients of calculating the propagation of extragalactic γ-rays and nucleons. We discuss the role and nature of the low energy photon background and the EGMF, and explain in detail the numerical method used in solving the transport equations. Section III is devoted to the treatment of the relevant interactions of γ-rays and nucleons. We compare our analysis with other work in Sec. IV. Section V discusses the generic forms of the injection spectra and the source distribution for a typical top-down model and the GRB scenario. Results and constraints from the spectra predicted at Earth are presented. In Sec. VI, I summarize the findings and discuss future prospects.

II. FORMALISM

A. Radiation backgrounds

UHE CRs undergo reactions with the universal diffuse radiation backgrounds permeating the universe [63]. The most relevant among them are the CMB, and the radio and IR-O backgrounds.

Photon primaries of energy E can be absorbed through pair production with a background photon of energy ϵ if ($c = \hbar = 1$ throughout)

$$E \geqslant E_{\text{th}} \equiv \frac{m_e^2}{\epsilon} = 2.611 \times 10^{11} \left(\frac{\epsilon}{1 \text{ eV}} \right)^{-1} \text{ eV}. \tag{1}$$

Therefore, for a typical CMB photon ($\epsilon \sim 10^{-3}$ eV) the threshold energy E_{th} is $\sim 3 \times 10^{14}$ eV, whereas for a typical radio photon ($\epsilon \lesssim 10^{-8}$ eV) the threshold is $\gtrsim 3 \times 10^{19}$ eV, thus affecting UHE γ-rays. Furthermore, since the pair production cross section peaks near the threshold, pair production on the radio background dominates over pair production on the CMB in that energy range although the number density of radio background photons is much smaller than that of CMB photons. On the other hand, the IR-O background affects the lower energy photons for the same reason. The threshold for pair production on the IR-O background lies at about $10^{12} - 10^{13}$ eV. Similarly, the contribution of the IR-O background to the total photopion production rate by protons is not negligible in the lower energy range ($E \lesssim 10^{18}$ eV).

All these backgrounds evolve with time (i.e. redshift), cooling with the expansion of the universe. However, on top of it, the radio background and the IR-O background evolve due to the evolution of the respective sources. The evolution of the radio background is tied to the evolution of the radio sources such as radio galaxies, and the evolution of the IR-O background to that of normal galaxies. Treating the evolution of these backgrounds carefully is important if we are to go back to the redshift where there existed not many of these sources ($z \gtrsim 5-6$). The flux of an isotropic radiation background component produced by an ensemble of identical sources is given by the following relation:

$$j(\epsilon, z) = \int_z^{z_i} \left(\frac{1+z}{1+z'} \right)^3 \Phi \left(\epsilon \frac{1+z'}{1+z}, z' \right)$$

$$\times \frac{1+z'}{1+z} \frac{c}{H_0} (1+z')^{-5/2} dz', \tag{2}$$

where $j(\epsilon, z)$ is the radiation flux (in units of number per area per time per solid angle per energy) at redshift z, z_i is the initial redshift when the sources begin to appear, H_0 is the Hubble constant, and $\Phi(\epsilon, z)$ is the production spectrum of the relevant background (in units of number of background photons per volume per time per solid angle per energy) at redshift z. Throughout this paper we assume $H_0 = 75$ km sec^{-1} Mpc^{-1} and a critical density universe (i.e. $\Omega_0 = 1$) for simplicity, but we keep H_0 in the formulas to show the dependence. If we assume that

$$\Phi(\epsilon, z) = \Phi_0(\epsilon)(1+z)^3 N_c(z), \tag{3}$$

where $\Phi_0(\epsilon)$ is the typical intensity spectrum of an individual source and $N_c(z)$ is the comoving density of the sources as a function of the redshift, Eq. (2) may be rewritten as

$$j(\epsilon, z) = \frac{c}{H_0} (1+z)^2 \int_z^{z_i} (1+z')^{-3/2}$$

$$\times \Phi_0 \left(\epsilon \frac{1+z'}{1+z} \right) N_c(z') dz'. \tag{4}$$

The background photon number density is then obtained from the relation $n(\epsilon, z) = 4\pi/c \cdot j(\epsilon, z)$. Note that it is important to self-consistently derive the background in this way rather than following the often-used approach of assuming a current background photon distribution, $n_0(\epsilon)$, and then extrapolating it back to higher redshifts via the formula $n(\epsilon, z) = (1+z)^2 n_0[\epsilon/(1+z)]$. While easy to implement, this approach is only valid for a truly primordial background formed at extremely high redshifts (e.g. the CMB) and can lead to misleading results if one is not careful.

The role of the IR-O background in determining the level of the cascade radiation background below ~ 1 TeV which is the diffuse γ-ray background due to cascades by CRs was examined in more detail in Ref. [64]. Even for rather extreme assumptions for the IR-O background, the cascade background level typically does not vary by more than a factor of a few. Accordingly, for this paper we have chosen to adopt a simple, ''middle of the road'' model for the formation of the IR-O background (a discussion of the various possibilities can be found in Refs. [65,66]). We assumed that the dominant contribution to the IR-O background comes from ordinary galaxies which formed early in the universe, at $z_i \simeq 5$. The typical galaxy was assumed to have a spectrum like that of the 5 Gyr disk galaxy spectrum shown in Fig. 4 of Ref. [67], which has a component peaking at $\simeq 1$ μm in wavelength due to direct emission from stars and a second component peaking at $\simeq 100$ μm due to reprocessing of the starlight by interstellar dust. The combined number and luminosity evolution of the galaxies was taken to go as $(1+z)^7$, i.e. most of the background was produced in a strong, initial burst of star formation in the galaxies, and the intensity of their emission was adjusted to give an optical background density today of $n_{\text{opt}} \simeq 2 \times 10^{-3}$ cm^{-3}.

For the present diffuse extragalactic radio background spectrum we use the estimate given in Ref. [68] (see also Refs. [63,69]). This spectrum can be parametrized by a power law with a lower frequency cutoff for which we use $f_c = 2$ MHz. One can also estimate the contribution to this background in the power law regime caused by radio galaxies. We did that by inserting the injection flux $\Phi(\epsilon, z)$ resulting from the radio luminosity function given by Eq. (7) of Ref. [70] into Eq. (2). The intensities resulting at $z = 0$ are within a factor $\simeq 2$ of the estimate given in Ref. [68]. We adopt the functional redshift dependence for the power law regime following from this calculation and normalize it to the present intensities given in Ref. [68]. In addition, we assume a redshift-independent lower frequency cutoff at $f_c = 2$ MHz.

The combined radiation spectrum at $z = 0$ used in this paper is presented in Fig. 1. In Fig. 2 we plot $N_c(z)$, i.e. the
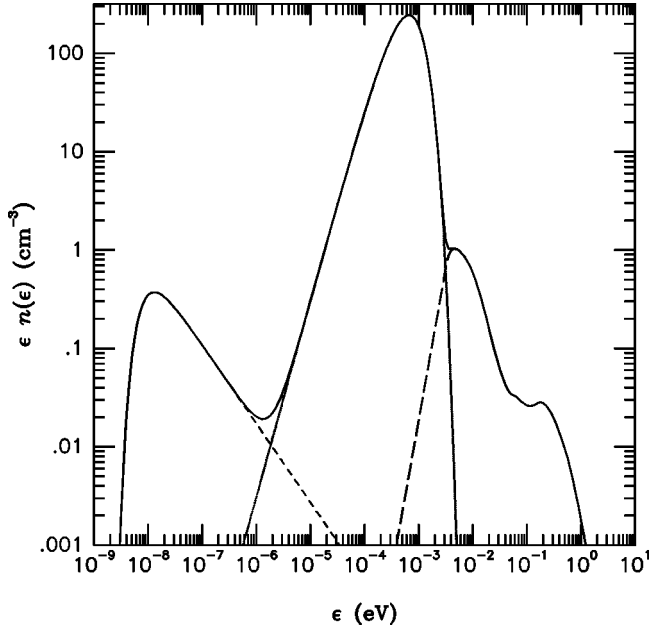
FIG. 1. The universal background radiation intensity spectrum at $z=0$ (solid line) used in our model. The separate contributions from the radio (short dashed line), the IR-O (long dashed line) background, and the CMB (dotted line) are also shown.
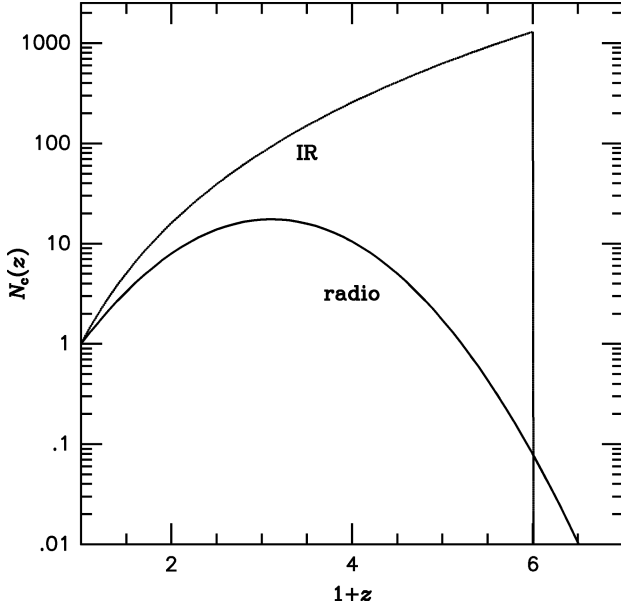
effective comoving densities of radio and IR-O sources whose luminosities are normalized at $z=0$, as functions of redshift.

B. Extragalactic magnetic field

The long range EGMF affects the propagation of CR particles via synchrotron radiation and deflection (or even diffusion).

FIG. 2. The effective comoving density of radio and IR-O sources whose luminosities are normalized at $z=0$, as a function of redshift. This corresponds to $N_c(z)$ in Eq. (3). The IR-O source density is assumed to cut off at $z=5$.

Synchrotron radiation is much more straightforward to consider than deflection. The synchrotron loss rate for a charged particle with mass m, energy E, and charge qe (e is the electron charge) subject to a magnetic field of strength B is given by [71]

$$\frac{dE}{dt} = -\frac{4}{3}\sigma_T \frac{B^2}{8\pi}\left(\frac{qm_e}{m}\right)^4\left(\frac{E}{m_e}\right)^2,\qquad(5)$$

where σ_T is the Thomson cross section, and m_e is the electron mass. Here, the average over random magnetic field orientations was taken. Synchrotron loss influences the electronic component of the cascade most strongly in the UHE regime [54]. On the other hand, at a given energy the synchrotron loss rate for protons is much smaller than that for electrons because the loss rate is proportional to m^{-4}. Thus, for protons synchrotron loss is completely negligible for the energies, magnetic field values, and distances we consider in this paper.

The relevant synchrotron power spectrum radiated by the electrons is given by [71]

$$\frac{dP}{dE_\gamma} = \frac{\sqrt{3}}{2\pi}\frac{e^3 B}{m_e}G(E_\gamma/E_c),\qquad(6)$$

where

$$G(x)\equiv x\int_x^\infty \sqrt{1-(x/\xi)^2}K_{5/3}(\xi)d\xi,\qquad(7)$$

and the critical energy E_c is defined as

$$E_c\equiv\frac{3eB}{2m_e}\left(\frac{E_e}{m_e}\right)^2\simeq 2.2\times10^{14}\left(\frac{E_e}{10^{21}\ \mathrm{eV}}\right)^2\left(\frac{B}{10^{-9}\ \mathrm{G}}\right)\ \mathrm{eV}.\qquad(8)$$

The power spectrum peaks at $E_\gamma\simeq0.23E_c$. The number spectrum, which is obtained by dividing Eq. (6) by the photon energy E_γ, is a monotonically decreasing function of energy.

Deflection is another important factor when dealing with the propagation problem in general [54]. The straight line propagation (SLP) approximation which treats the motion of CR particles in one dimension fails if the effect of the deflection becomes large. The gyroradius of a charged particle with charge qe and momentum p (energy E) is given by

$$R_g = \frac{p}{qeB_\perp}\simeq\frac{E}{qeB_\perp}\simeq1.1\times10^3\frac{1}{q}\left(\frac{E}{10^{21}\ \mathrm{eV}}\right)$$

$$\times\left(\frac{B_\perp}{10^{-9}\ \mathrm{G}}\right)^{-1}\ \mathrm{Mpc},\qquad(9)$$

where $B_\perp$ is the field component perpendicular to the particle's motion. Note that the EGMF deflects protons and electrons by the same amount at a given energy once they are relativistic. If the gyroradius of a charged particle is considerably longer than the source distance, the effect of the deflection is practically negligible. On the other hand, if the gyroradius is comparable or shorter than the source distance,
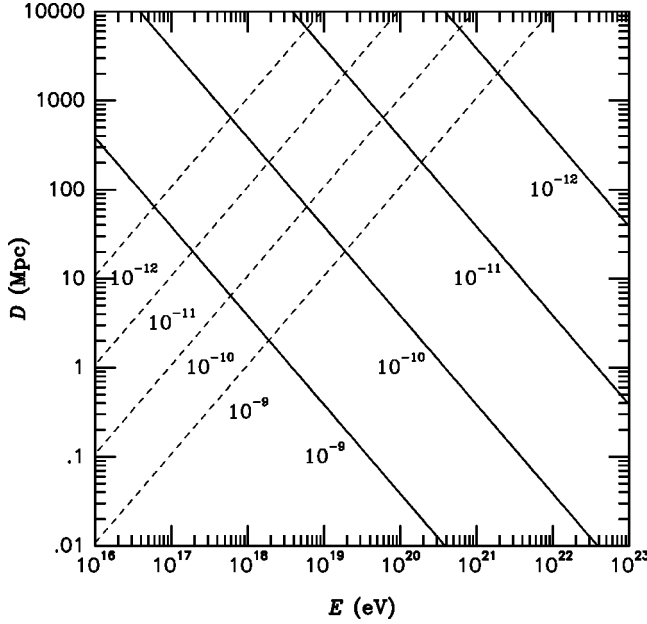
FIG. 3. Gyroradii (dashed lines) and synchrotron loss lengths (solid lines) of electrons for various strengths of the EGMF in units of gauss (G) as indicated.

the deflection may not be neglected and one now has to keep track of the transversal motion, which makes the problem much more complicated. However, if the sources are distributed homogeneously and isotropically throughout the universe, then the influence of the deflection on the shape of the spectrum becomes small. Although this is a purely mathematical model, it is a good approximation for many realistic situations. On the other hand, if one considers the CR flux from a single source, deflection becomes important.

In the case of an EM cascade the propagating particle basically alternates between a photon and an electron, and only electrons are affected by the EGMF. Therefore, the effective gyroradius of a cascade photon R_g^γ can be expressed as

$$R_g^\gamma \simeq R_g^{e^-}\left(1+\frac{L_\gamma}{L_e}\right),\qquad(10)$$

where $R_g^{e^-}$ is the electron gyroradius, L_γ is the photon interaction length, and L_e is the energy loss length for the electron. If the effective gyroradius is considerably shorter than the source distance, the real spectrum would be very different from what one obtains by using the SLP assumption, and below the energy where the gyroradius is comparable to the source distance the flux is expected to be heavily suppressed. This point has been ignored in most of the work on CR propagation [47,48,52]. Figure 3 illustrates the gyroradii and the synchrotron loss rates of electrons for various strengths of the EGMF. In this paper, the strength of the EGMF is assumed as a free parameter between 0 and 10^{-9} G as in Ref. [54].

C. Transport equations

We adopt a transport equation scheme to solve the propagation problem. Since we have an EM cascade ensuing, it is inadequate to use the simple continuous energy loss (CEL) approximation which neglects non-leading particles. In addition, since particle numbers grow fast with time, using a full-blown Monte Carlo calculation will require excessive computing time. In this problem, using the transport equation approach is very economical in terms of computing time as well as sufficiently accurate. Previous work done by Protheroe and Johnson [52] uses a mixture of transport equations and Monte Carlo techniques.

A sample transport equation for electrons which includes pair production (PP) and inverse Compton scattering (ICS) can be written as follows:

$$\frac{d}{dt}N_e(E_e,t)=-N_e(E_e,t)\int d\epsilon\,n(\epsilon,t)$$

$$\times\int d\mu\,\frac{1-\beta_e\mu}{2}\sigma_{ICS}(E_e,\epsilon,\mu)$$

$$+\int dE_e'N_e(E_e',t)\int d\epsilon\,n(\epsilon,t)$$

$$\times\int d\mu\,\frac{1-\beta_e'\mu}{2}\frac{d\sigma_{ICS}}{dE_e}(E_e;E_e',\epsilon,\mu)$$

$$+\int dE_\gamma N_\gamma(E_\gamma,t)\int d\epsilon\,n(\epsilon,t)$$

$$\times\int d\mu\,\frac{1-\mu}{2}\frac{d\sigma_{PP}}{dE_e}(E_e;E_\gamma,\epsilon,\mu)+Q(E_e,t),$$

$$(11)$$

where $N_e(E_e,t)$ is the (differential) number density of electrons at energy E_e at time t, $n(\epsilon,t)$ is the number density of background photons at energy ϵ at time t, $Q(E_e,t)$ is an external source term for electrons at energy E_e at time t, μ is the cosine of the interaction angle between the CR electron and the background photon ($\mu=-1$ for a head-on collision), and β_e is the velocity of the CR electron. The terms describe the loss of electrons due to ICS, the influx of electrons scattered into the energy range due to ICS, the influx of electrons produced due to PP by photons, and the external injection. The factor $(1-\beta_e\mu)/2$ is the flux factor. We define the angle averaged cross sections $R(E,\epsilon)$ and $P(E';E,\epsilon)$ as

$$R(E,\epsilon)\equiv\int d\mu\,\frac{1-\beta\mu}{2}\sigma(E,\epsilon,\mu),\qquad(12)$$

and

$$P(E';E,\epsilon)\equiv\int d\mu\,\frac{1-\beta\mu}{2}\frac{d\sigma}{dE'}(E';E,\epsilon,\mu).\qquad(13)$$

Then Eq. (11) is rewritten as

$$\frac{d}{dt}N_e(E_e,t) = -N_e(E_e,t)\int d\epsilon\, n(\epsilon,t)R_{\text{ICS}}(E_e,\epsilon)$$

$$+\int dE_e' N_e(E_e',t)$$

$$\times\int d\epsilon\, n(\epsilon,t)P_{e,\text{ICS}}(E_e;E_e',\epsilon)$$

$$+\int dE_\gamma N_\gamma(E_\gamma,t)$$

$$\times\int d\epsilon\, n(\epsilon,t)P_{e,\text{PP}}(E_e;E_\gamma,\epsilon)$$

$$+Q(E_e,t). \tag{14}$$

In order to solve this differential equation numerically, we first bin the energies of the CR electrons, CR photons, and background photons. We divide each decade of energy into 20 equidistant logarithmic bins and call the central value of the i-th bin E_i and boundary values $E_{i-1/2}$ and $E_{i+1/2}$. And we replace the continuous integrals by finite sums, and integrate Eq. (14) over one CR energy bin. Then we get

$$\frac{d}{dt}N_e^k = -N_e^k\sum_j \Delta\epsilon_j n(\epsilon_j)R_{\text{ICS}}^{kj}$$

$$+\sum_i \sum_j N_e^i \Delta\epsilon_j n(\epsilon_j)P_{e,\text{ICS}}^{ijk}$$

$$+\sum_i \sum_j N_\gamma^i \Delta\epsilon_j n(\epsilon_j)P_{e,\text{PP}}^{ijk}+Q^k, \tag{15}$$

where $N^i\equiv\int_{E_{i-1/2}}^{E_{i+1/2}}dE\,N(E,t)$, $R^{kj}\equiv R(E_k,\epsilon_j)$, $P^{ijk}\equiv\int_{E_{k-1/2}}^{E_{k+1/2}}dE\,P(E;E_i,\epsilon_j)$, $Q^i\equiv\int_{E_{i-1/2}}^{E_{i+1/2}}dE\,Q(E,t)$, and $\Delta\epsilon_j\equiv\epsilon_{i+1/2}-\epsilon_{i-1/2}$.

We adopt a first order implicit scheme to solve this difference equation (15); i.e.

$$N_e^{k\prime}=\frac{\frac{1}{\Delta t}N_e^k+\Sigma_{i\neq k}\Sigma_j N_e^{i\prime}\Delta\epsilon_j n(\epsilon_j)P_{e,\text{ICS}}^{ijk}+\Sigma_{i,j}N_\gamma^{i\prime}\Delta\epsilon_j n(\epsilon_j)P_{e,\text{PP}}^{ijk}+Q^k}{\frac{1}{\Delta t}+\Sigma_j\Delta\epsilon_j n(\epsilon_j)(R_{\text{ICS}}^{kj}-P_{e,\text{ICS}}^{kjk})}, \tag{16}$$

where $N_e^{k\prime}$ is a solution advanced by a timestep Δt from N_e^k. Equation (16) can be understood as follows: the second term in the denominator corresponds to the *net* loss of the particles from bin k. The second term in the numerator corresponds to the net *scattered* particle influx into bin k due to scattering from other bins which conserves the particle species. The third and the last terms in the numerator describe the influx of the particles due to production by different particles and due to external injection. Various different interactions can be included in this main equation according to the general scheme laid out above, including certain energy losses which can be treated as continuous such as synchrotron radiation for which we use a simple first order upwind scheme.

The implicit method has the advantage that the solution converges for arbitrary size of the timestep we take. Therefore, we are allowed to use a bigger timestep than is allowed by an explicit Euler scheme. However, to ensure the desired accuracy, we need to optimize the stepsize for a given problem by trial and error.

It is important to monitor conservation of particle numbers and total energy in order to obtain reliable results. For example, for ICS the coefficients should satisfy

$$R^{ij}=\sum_k P_e^{ijk}=\sum_k P_\gamma^{ijk} \quad \text{(number)} \tag{17}$$

and

$$(E_i+\epsilon_j)R^{ij}=\sum_k E_k P_e^{ijk}+\sum_k E_k P_\gamma^{ijk} \quad \text{(energy)}. \tag{18}$$

It is sometimes necessary to adjust the coefficients in order to obey these relations. This stabilizes the calculation against growing errors due to discretization of variables.

In Eq. (16) the coefficient matrices are multiplied with and summed over the background photon spectrum vector and/or the CR spectrum vector at a given redshift in order to advance the solution. This procedure has the advantage that one can deal with an arbitrary evolution of the radiation backgrounds in time, which is important in this problem. If one would integrate the background spectrum into the coefficients beforehand, it would become extremely difficult and time-consuming to handle an arbitrary background evolution because one would have to obtain the coefficients by integration at *each* redshift.

In Ref. [52], it was assumed that all radiation backgrounds exhibit a trivial evolution by redshifting. This allowed them to adopt a matrix doubling method [72] for the propagation calculations. However, in case of a more realistic background evolution, matrix doubling is almost impossible. In contrast, our approach is always guaranteed to work efficiently and is sufficiently accurate in the more general case.

Equation (16) is then solved iteratively by inserting the initial values for $N^{i\prime}$'s on the right hand side and re-inserting

the new values until a convergence is achieved. Since there are four main particle species (nucleons, photons, electrons, and neutrinos), one should converge all spectra simultaneously. However, it is economical and equally valid to converge each particle spectrum separately while holding the others fixed, and repeat this whole procedure until all spectra converge.

In addition, we account for redshifting by performing the operation $N_a(E,z) \to [1 + \Delta z/(1+z)]^{-2} N_a(E[1+\Delta z/(1+z)],z)$ for each particle species a after a step Δz in redshift. Here we match Δz conveniently with the logarithmic energy bin size, $\log_{10}[1+\Delta z/(1+z)] = \log_{10}(E_i/E_{i-1}) = 1/20$, which corresponds to the transformation $N_a^i(z) \to [1+\Delta z/(1+z)]^{-3} N_a^{i+1}(z)$.

The numerical code is developed by the author, Paolo Coppi, and Günter Sigl.

III. INTERACTIONS OF RELATIVISTIC NUCLEONS AND γ-RAYS

In this section we discuss various relevant interactions and their cross sections from which the coefficients R and P used in the transport equations are calculated.

A. "Cascade" photons

Pair production (PP) and inverse Compton scattering (ICS) are the two main processes that drive the EM cascade. First, let us define the inelasticity which is the fraction of the energy that is transferred from the scattering particle to the scattered (or produced). It is given by

$$\eta(s) \equiv 1 - \frac{1}{\sigma_{\text{tot}}(s)} \int d\epsilon' \epsilon' \frac{d\sigma}{d\epsilon'}(\epsilon',s), \qquad (19)$$

where s is the squared center of mass (c.m.) energy and ϵ' is the energy of the recoiling (leading) particle in units of the initial particle energy.

In the extreme Klein-Nishina limit where $s \gg m_e^2$, one particle in an electron-positron pair produced in a pair production event typically carries exclusively almost all of the initial total energy. The produced high energy electron (positron) then undergoes ICS, and the inelasticity for ICS in this high energy limit is more than 90%. Therefore, $e^-(e^+)$ loses most of its energy and the background photon is upscattered with almost all of the initial energy of the UHE photon. This cycle of the "cascade" photon is responsible for slowing down the energy attenuation of the leading particle. In some previous work it was incorrectly claimed that the UHE photons lose energy very fast based on the fact that the *mean free path* of the UHE photon is fairly short, but this sequence of PP and ICS makes the actual energy attenuation much slower. In addition, the contribution of non-leading particles to the flux which are neglected in the CEL approximation can be substantial for cascades which are not fully developed. This will be important in some of the applications considered in this paper.

If the EGMF is present, however, the above scenario changes somewhat. In the energy range where the synchro-

tron loss rate for the electrons is greater than the ICS rate, the development of the EM cascade is heavily suppressed. Its penetration depth is basically reduced to the photon mean free path in this energy regime. A more detailed discussion is found in Ref. [54].

1. Pair production

The total cross section for PP ($\gamma\gamma_b \to e^- e^+$) is well-known and is given by

$$\sigma_{\text{PP}} = \sigma_T \cdot \frac{3}{16}(1-\beta^2)\left[(3-\beta^4)\ln\frac{1+\beta}{1-\beta} - 2\beta(2-\beta^2)\right], \qquad (20)$$

where $\beta \equiv (1-4m_e^2/s)^{1/2}$ is the velocity of the outgoing electron in the c.m. frame. In order to calculate the differential cross section, we adopt the simplifying approximation where the dependence of the cross section on the azimuthal angle of the outgoing particle in the CR frame is ignored. Since the terms that depend on the azimuthal angle are smaller by more than 10^{-11} than the leading order terms, this approximation is very accurate for practical purposes. The differential cross section for a photon of energy E_γ to produce an electron of energy E_e' is then given by [73,74]

$$\frac{d\sigma_{\text{PP}}}{dE_e'} = \sigma_T \cdot \frac{3}{4} \frac{m_e^2}{s} \frac{1}{E_\gamma}\left[\frac{E_e'}{E_\gamma - E_e'} + \frac{E_\gamma - E_e'}{E_e'}\right.$$
$$+ E_\gamma(1-\beta^2)\left(\frac{1}{E_e'} + \frac{1}{E_\gamma - E_e'}\right)$$
$$\left. - \frac{E_\gamma^2(1-\beta^2)^2}{4}\left(\frac{1}{E_e'} + \frac{1}{E_\gamma - E_e'}\right)^2\right], \qquad (21)$$

where the range is restricted to $(1-\beta)/2 \leq E_e'/E_\gamma \leq (1+\beta)/2$. The differential cross section with respect to the positron energy is identical due to symmetry.

2. Double pair production

Double pair production (DPP; $\gamma\gamma_b \to e^- e^+ e^- e^+$) is a higher order QED process that affects the UHE photons. It is known that the DPP total cross section is a sharply rising function of s at the threshold and approaches the asymptotic value quickly at $\sigma(\infty) \approx 6.45 \ \mu$b [75]. For interactions with the microwave background, the DPP rate begins to dominate over the PP rate above $\sim 10^{21}$ eV. If we take the contribution of the radio background into account, this energy goes up somewhat.

The differential cross sections of DPP may be obtained through second order QED calculations, but it is extremely involved, and we could not find a suitable reference in which the differential cross section is calculated. In addition, since it is still a small sized effect, we think that introducing a reasonable assumption about the differential cross section is adequate for our purpose. Therefore, we use the assumption where one pair of the two carries all the initial energy and two particles in the pair share the energy equally. We believe
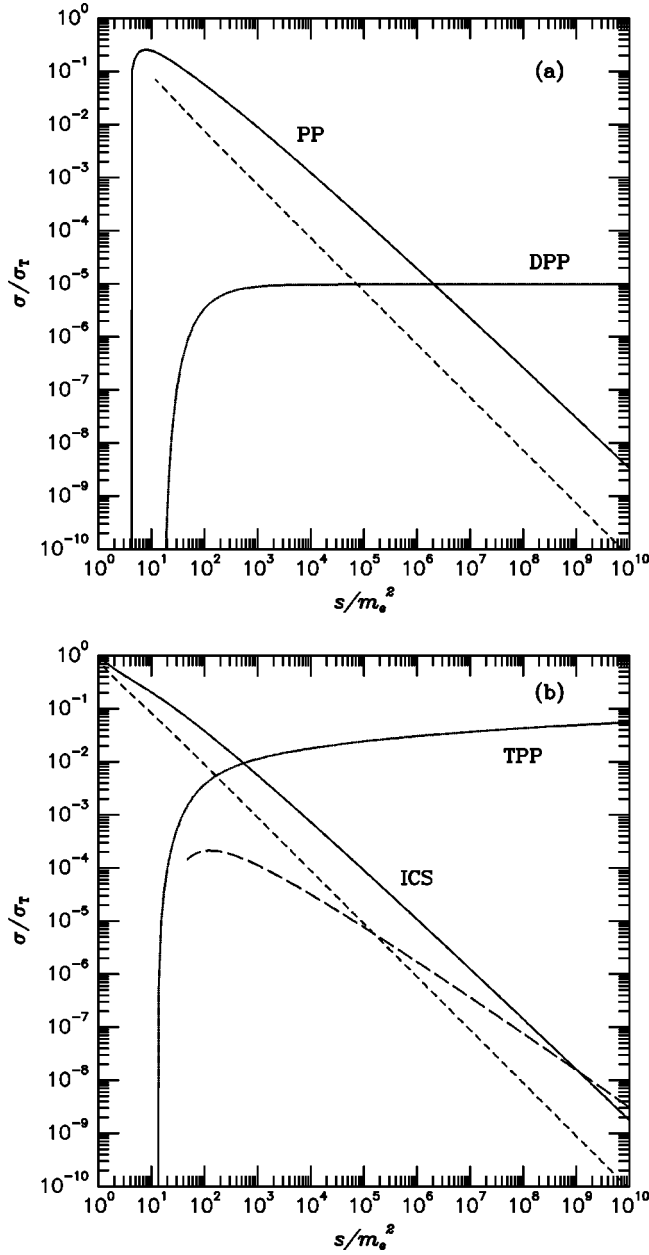
FIG. 4. The total cross sections, $\sigma(s)$, and the cross sections times the average inelasticity, $\sigma(s)\eta(s)$, which is proportional to the fractional energy loss rate of the leading particle: (a) For PP (solid line and short dashed line, respectively) and DPP (dotted line); (b) For ICS (solid line and short dashed line, respectively) and TPP (dotted line and long dashed line, respectively).

that this assumption does not change the calculations in a significant way.

In Fig. 4(a) we plot $\sigma(s)$ and $\sigma(s)\eta(s)$, the latter of which is proportional to the fractional energy loss rate of the leading particle, for PP and DPP.

3. Inverse Compton scattering

The total cross section for ICS ($e\gamma_b \rightarrow e\gamma$) is given by the well-known Klein-Nishina formula:

$$\sigma_{\text{ICS}} = \sigma_T \cdot \frac{3}{8} \frac{m_e^2}{s\beta} \left[\frac{2}{\beta(1+\beta)}(2+2\beta-\beta^2-2\beta^3) \right.$$

$$\left. -\frac{1}{\beta^2}(2-3\beta^2-\beta^3)\ln\frac{1+\beta}{1-\beta} \right], \qquad (22)$$

where $\beta \equiv (s-m_e^2)/(s+m_e^2)$ is the velocity of the outgoing electron in the center of mass frame. Most part of the energy range of interest is in the extreme Klein-Nishina regime, but nonetheless we use the exact formula.

The differential cross section for an electron of energy E_e to produce an electron of energy E_e' is then given by [73,74]:

$$\frac{d\sigma_{\text{ICS}}}{dE_e'} = \sigma_T \cdot \frac{3}{8} \frac{m_e^2}{s} \frac{1}{E_e} \frac{1+\beta}{\beta} \left[\frac{E_e'}{E_e} + \frac{E_e}{E_e'} + \frac{2(1-\beta)}{\beta}\left(1-\frac{E_e}{E_e'}\right) \right.$$

$$\left. + \frac{(1-\beta)^2}{\beta^2}\left(1-\frac{E_e}{E_e'}\right)^2 \right], \qquad (23)$$

where the range is restricted to $(1-\beta)/(1+\beta) \lesssim E_e'/E_e \leqslant 1$. The differential cross section with respect to the energy E_γ' of the outgoing photon is obtained by substituting $E_e - E_\gamma'$ for E_e' in Eq. (23).

4. Triplet pair production

Triplet pair production (TPP; $e\gamma_b \rightarrow ee^-e^+$) is a rather significant contribution to the interactions of UHE electrons. This process is discussed in detail in Refs. [76–78]. Although the total cross section for TPP on CMB photons becomes comparable to the ICS cross section already at $\sim 10^{17}$ eV, the actual energy attenuation is not important until much higher energies because the inelasticity is very small ($\lesssim 10^{-3}$). Nonetheless, it is fairly efficient in channelling the energy content to lower energies, and may not be ignored.

We use the formulation given by [77] in calculating the total cross section, and the detailed expressions are given in Appendix A. The total cross section of TPP increases asymptotically logarithmically with s:

$$\sigma_{\text{TPP}} = \sigma_T \frac{3\alpha}{8\pi} \left[\frac{28}{9}\ln\frac{s}{m_e^2} - \frac{218}{27} \right] \quad (s \gg m_e^2), \qquad (24)$$

where α is the fine structure constant.

While it is possible to calculate the differential cross sections numerically using the expressions given in Ref. [76–78], it is extremely time-consuming because it involves multi-dimensional integrations of very complicated functions. Furthermore, some of the variables introduced there become very large or very small, and hence create problems with the finite computing precision. The detailed behavior of the TPP cross sections near threshold is unimportant since TPP is dominated by ICS in this energy regime. Thus, it will suffice to use a simple and efficient approximation that works very well for the region away from the threshold. First, we make note of the fact that the differential cross section with respect to the energy of one of the particles of

the produced pair tends to $d\sigma/dE' \propto E'^{-7/4}$ for $s \gg m_e^2$ [76]. Furthermore, in the same regime the inelasticity for TPP can be well approximated by [76]

$$\eta(s) \simeq 1.768(s/m_e^2)^{-3/4}. \qquad (25)$$

We then make the assumption that the differential rate $P(E';E,\epsilon)$ for the produced particle with energy E' and for the incoming electron with energy E and the incoming background photon with energy ϵ is given as a power law with spectral index δ:

$$P(E';E,\epsilon) = R(E,\epsilon)C(E,\epsilon)E'^{-\delta}, \qquad (26)$$

where $C(E,\epsilon)$ is a normalization factor. Then using the requirement that the integrated differential rates must be the same as the total rate and energy conservation [i.e. the analogues of Eqs. (17) and (18)], one can uniquely determine the coefficient $C(E,\epsilon)$ and δ. The spectral index δ obtained this way does approach 7/4 for large s.

For the recoiling electron, on the other hand, we may assume continuous energy loss whose rate is given by

$$\frac{dE}{dt} \simeq -E \int d\epsilon\, n(\epsilon)R(E,\epsilon)\eta(s). \qquad (27)$$

The importance of TPP again depends on the presence and the strength of the EGMF. If the EGMF is stronger than about 10^{-12} G, then TPP energy loss is dominated by synchrotron cooling, and it is no longer very important. Since various arguments and indirect measurements of the EGMF [79] suggest that EGMF is at least 10^{-12} G, TPP may not play a big role in the propagation of UHE photons. However, in the absence of the EGMF, the contribution of TPP to the energy attenuation of electrons and photons is comparable to or even greater than ICS above $\sim 10^{22}$ eV and thus may not be ignored.

In Fig. 4(b) we plot $\sigma(s)$ and $\sigma(s)\eta(s)$ of which the latter is proportional to the fractional energy loss rate of the "leading particle," for ICS and TPP. Figure 5 shows all the rates at redshift $z=0$ that affect the photons and electrons in the energy range we consider.

5. Other processes

Other interactions that are neglected in this paper are all processes involving the production of one or more e^-e^+ pairs substituted by muon, tau lepton, and pion pairs, double Compton scattering ($e\gamma_b \to e\gamma\gamma$), $\gamma\gamma$ scattering ($\gamma\gamma_b \to \gamma\gamma$), Bethe-Heitler pair production ($\gamma X \to Xe^+e^-$, where X can be an atom, an ion, or a free electron), the process $\gamma\gamma_b \to e^+e^-\gamma$, and pair production on a magnetic field ($\gamma B \to e^-e^+$). The total cross section of single muon pair production ($\gamma\gamma_b \to \mu^-\mu^+$), for example, is smaller than electron pair production by about a factor of 10. Energy loss rates for TPP involving heavier pairs are suppressed by a factor $\simeq (m/m_e)^{1/2}$ in the limit of large s. Similarly, double pair production involving heavier pairs is also negligible [75]. The double Compton scattering cross section is of order α^3 and must be treated together with the radiative correc-
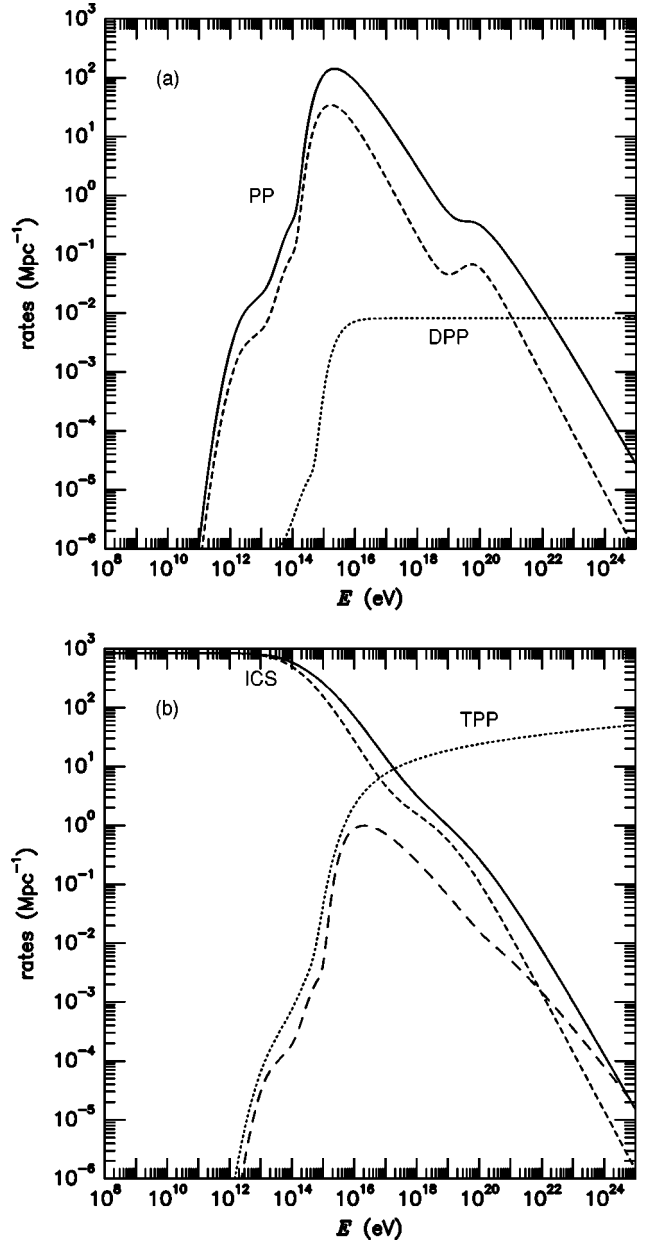

FIG. 5. The relevant interaction rates at $z=0$ that affect the photons and electrons in the energy range we consider. The keys are identical to those for Fig. 4. The rates are calculated by folding the total cross sections and inelasticity weighted cross sections with the present background photon spectrum shown in Fig. 2.

tions to ordinary Compton scattering of the same order. The corrections to the lowest order ICS cross section by processes involving m_γ additional photons in the final state, $e\gamma_b \to e+(m_\gamma+1)\gamma$, $m_\gamma \geq 1$, turn out to be less than 10% in the energy range under consideration [80]. A similar remark applies to corrections to the lowest order PP cross section by the processes $\gamma\gamma_b \to e^+e^- + m_\gamma\gamma$, $m_\gamma \geq 1$. Photon-photon scattering can only play a role for $z \gtrsim 100$ and energies below the redshift-dependent pair production threshold Eq. (1) [81, 82]. A similar remark applies to Bethe-Heitler pair production on atoms, ions and free electrons [82]. Pair production on a magnetic field of order 10^{-6} G which is typical for the

field of our galaxy, is only relevant for $E \gtrsim 10^{24}$ eV. This critical energy is even higher for the EGMF and this process is thus negligible in the analysis.

B. Nucleons

There are three major processes that affect the propagation of protons and neutrons: Electron-positron pair production by protons (PPP; $p\gamma_b \rightarrow pe^-e^+$), photopion production [$N\gamma_b \rightarrow N(n\pi)$, $n \geq 1$], and neutron β-decay ($n \rightarrow pe^-\bar{\nu}_e$).

1. Pair production by protons

PPP provides the main energy attenuation for protons with energies below the GZK cutoff [83]. The energy threshold for this process is

$$E_{\text{th}} = \frac{m_e(m_N + m_e)}{\epsilon} \simeq 4.8 \times 10^{14} \left(\frac{\epsilon}{\text{eV}} \right)^{-1} \quad \text{eV}. \quad (28)$$

Thus, for a microwave background photon ($\epsilon \sim 10^{-3}$ eV), PPP ensues at a proton energy $E \sim 5 \times 10^{17}$ eV. Below this energy, the protons cool essentially only by redshifting with the expansion.

The PPP total cross section behaves very similarly to that for triplet pair production because PPP is almost identical to TPP [84], and the expression for the total cross section away from the threshold may be given by Eq. (24). However, while TPP near its threshold is dominated by other processes, the exact behavior of PPP rates near the threshold is important because PPP dominates the proton energy loss in that energy range. We use the parametric fits given in Ref. [85] for the cross section and inelasticity. Then we use the same approach in calculating the differential rates as we did for TPP. It can be shown that these rates are well approximated by a power law. On the other hand, the proton spectrum evolution due to PPP is well described by CEL because the inelasticities are smaller than 10^{-3} at all relevant energies. Production of heavier pairs like $\mu^+\mu^-$ is suppressed similarly to the case of TPP. The energy ranges for the produced pairs and the recoiling proton are given in Appendix A.

2. Photopion production

Photopion production provides the main energy attenuation for nucleons above $E \simeq 10^{19}$ eV. The energy threshold for this process is

$$E_{\text{th}} = \frac{m_N m_\pi + m_\pi^2/2}{\epsilon} \simeq 6.8 \times 10^{16} \left(\frac{\epsilon}{\text{eV}} \right)^{-1} \quad \text{eV}. \quad (29)$$

Thus, for a microwave background photon ($\epsilon \sim 10^{-3}$ eV), photopion production ensues at a nucleon energy $E \sim 7 \times 10^{19}$ eV. Since publications on numerical studies of nucleon and γ-ray propagation usually do not contain detailed information on the implementation especially of multiple pion production, we present our approach here in some detail. First, we define a few suitable kinematic variables which depend only on the incoming particles. If E_γ^{lab} is the photon energy in the laboratory frame (LF) where the

nucleon is at rest, m_N is the nucleon mass, and s is the squared center of mass (c.m.) energy, then the following relations hold:

$$\kappa \equiv \frac{E_\gamma^{\text{lab}}}{m_N} = \frac{\epsilon E_N}{m_N^2}(1 - \mu),$$

$$s = m_N^2(1 + 2\kappa). \quad (30)$$

Since laboratory measurements of cross sections are usually given in terms of E_γ^{lab}, we conveniently express everything in terms of κ in the following.

Concerning single pion production we consider the following reactions:

$$\gamma + N \rightarrow \pi^0 + N: \frac{d\sigma_1}{d\Omega^*} = \sum_{j=0}^{K} a_{1j}(\kappa)(x^*)^j, \quad (31)$$

$$\gamma + p \rightarrow \pi^+ + n: \frac{d\sigma_2}{d\Omega^*} = (1 - \beta^*x^*)^{-1/2} \sum_{j=0}^{K} a_{2j}(\kappa)(x^*)^j, \quad (32)$$

$$\gamma + n \rightarrow \pi^- + p: \frac{d\sigma_3}{d\Omega^*} = (1 - \beta^*x^*)^{-1/2} \sum_{j=0}^{K} a_{3j}(\kappa)(x^*)^j. \quad (33)$$

The differential cross sections for these processes are expressed here in terms of κ and the c.m. quantities Ω^*, β^*, and x^* which denote solid angle, pion velocity, and the cosine of the scattering angle, respectively. The functions $a_{ij}(\kappa)$, $i = 1,2,3$ and $j = 1, \ldots, N$ are fitted to laboratory cross section data and we use fits up to order $K = 3$ [86]. The expressions in Eqs. (31)–(33) can be easily rewritten in terms of the energies of the outgoing nucleons and pions in the cosmic ray frame (CRF) which we denote by E_a' for $a = p, n, \pi^+, \pi^-, \pi^0$. The relevant formulas are given in Appendix B.

Note that in Eq. (31) we have assumed identical cross sections for the two charge retention processes involving protons and neutrons. This is a very good approximation (see, e.g. Ref. [86]). Reactions (32) and (33) constitute the charge exchange reactions for single pion production.

We now turn to multiple pion production. At this point, it is worthwhile noting the following fact. Although the energy of the cosmic ray nucleons considered in the study reaches up to 10^{25} eV which is close to the supersymmetric energies, the actual center of mass energy for multiple pion production that take place is not extremely high. This is because that the energy of the interacting background photons is very low. For example, for the interaction with the CMB photons, the center of mass energy of multiple pion production by a nucleon with energy 10^{24} eV is still only tens of GeV. Therefore, it is usually not necessary to consider higher order QCD effects rigorously. Furthermore, in most cosmic ray production scenarios, multipion production never becomes a deciding factor because the maximum energy of nucleons in most nucleon-dominated scenarios hardly reaches beyond the GZK cutoff at which single pion production is still dominant.

Thus, for our purpose a simplified approach to multipion production is sufficient and adequate.

Let us first consider the channel $\gamma + p \rightarrow \pi^- + X$ where X stands for anything. This channel has been discussed in detail in Ref. [87]. There, the Feynman x-variable $x = p_{\parallel}^*/p_{\max}^*$ was introduced, which is the fraction of the pion parallel momentum $p_{\parallel}^*$ in the CMF to its maximal value

$$p_{\max}^* = m_N \frac{D}{(1+2\kappa)^{1/2}}, \tag{34}$$

where $D \equiv [(\kappa - \varepsilon^2/2)^2 - \varepsilon^2]^{1/2}$, and $\varepsilon = m_\pi/m_N$ is the ratio of the pion and nucleon mass. Denoting the transverse momentum with $p_\perp$ and the π^- energy in the CMF by $E_{\pi^-}^*$, the differential cross section for π^- production was written in terms of a structure function $F(x, p_\perp^2, s)$:

$$d^2\sigma_{\gamma p \rightarrow \pi^- X} = \pi \frac{p_{\max}^*}{E_{\pi^-}^*} F(x, p_\perp^2, s) dx \, dp_\perp^2. \tag{35}$$

Performing Lorentz transformations into the CRF where the proton and π^- energies are E_p and E_{π^-}' (see Appendix B), this can be written as

$$\frac{d\sigma_{\gamma p \rightarrow \pi^- X}}{dE_{\pi^-}'} = \frac{2\pi m_N p_{\max}^*}{E_p} (1+2\kappa)^{1/2} \int_{x_{\min}}^{x_{\max}} dx$$

$$\times F\left[x, -m_\pi^2 + \left(\frac{E_{\pi^-}' - m_N}{E_N} \right)^2 (1+2\kappa) \right.$$

$$\left. + 2p_{\max}^* \left(\frac{E_{\pi^-}' - m_N}{E_N} \right) (1+2\kappa)^{1/2} x, s \right], \tag{36}$$

where $x_{\min} \geq -1$ is chosen such that $p_\perp^2 \geq 0$ which is the second argument of F, and $x_{\max}$ such that $p_\perp^2/(p_{\max}^*)^2 + x^2 \leq 1$.

We take into account only the processes above some threshold which is sufficiently high such that the contribution of single pion production is negligible; we take $\kappa \geq 2(\varepsilon + \varepsilon^2)$. Furthermore, whereas Ref. [87] states that the structure function F is independent of s, it is known that the total cross section increases roughly logarithmically in s [88]. Therefore, we assume here that the structure function depends on s through a factor $h(s)$, where $h(s)$ is set such that the integrated total cross section matches the measurement given in Ref. [88]. Finally, for our purposes we assume that F further factorizes into an x-dependent part and an exponential dependence on $p_\perp^2$:

$$F(x, p_\perp^2, s) \simeq \frac{1}{\Lambda^2} \exp[-p_\perp^2/\Lambda^2] f(x) h(s). \tag{37}$$

Here, $\Lambda \simeq \text{GeV}/6.4$ is roughly of the order of the QCD scale and $f(x)$ can be fitted to the data presented in Ref. [87]. We also note that the Feynman scaling is violated at very high energies, but in my opinion the use of the Feynman scaling is a good working approximation, and the addition of a scaling-violating term will not introduce significant changes in the results because it mainly affects the nucleons with energies

well into the multiple pion production regime and this will amount mainly to changes in the nucleon spectrum well above the GZK cutoff where the detailed form of the nucleon spectrum is relatively less important.

Within these approximations we have finally

$$\frac{d\sigma_4}{dE_{\pi^-}'} \equiv \frac{d\sigma_{\gamma p \rightarrow \pi^- X}}{dE_{\pi^-}'}$$

$$= \frac{2\pi}{E_p} \left(\frac{m_N}{\Lambda} \right)^2 D \int_{x_{\min}}^{x_{\max}} dx \, h(s) f(x)$$

$$\times \exp\left\{ -\left(\frac{m_N}{\Lambda} \right)^2 \left[-\varepsilon^2 + \left(\frac{E_{\pi^-}'}{E_p} \right)^2 \right. \right.$$

$$\left. \left. \times (1+2\kappa) + 2D\left(\frac{E_{\pi^-}'}{E_p} \right) x \right] \right\}, \tag{38}$$

where $x_{\min}$ and $x_{\max}$ are given by

$$x_{\min} = \max\left[-1, \frac{\varepsilon^2 - (E_{\pi^-}'/E_p)^2(1+2\kappa)}{2D(E_{\pi^-}'/E_p)} \right],$$

$$x_{\max} = -\frac{E_\pi'}{E_p} \frac{1+2\kappa}{D} + \left(1 + \varepsilon^2 \frac{1+2\kappa}{D^2} \right)^{1/2}. \tag{39}$$

At this point it is important to realize that $f(x) = f_c(x) + f_\rho(x)$ can be divided into a contribution $f_c(x)$ from the "central" pions and a contribution $f_\rho(x)$ from production of multiple ρ_0 mesons (sometimes also called the leading pion contribution) which subsequently decay into equal distributions of π^+ and π^-. Therefore, $f_\rho(x)$ exclusively contributes to the production of π^+ and π^- and corresponds to a charge retention process where the nature of the nucleon is unchanged. In contrast, $f_c(x)$ describes a process resulting in approximately equal production of π^0 and π^- with the probability for change of nucleon isospin being about 2/5 (from simple quark counting). From these assumptions it follows immediately that $d\sigma_5/dE_{\pi^0}' \equiv d\sigma_{\gamma p \rightarrow \pi^0 X}/dE_{\pi^0}'$ is obtained by substituting $f_c(x)$ for $f(x)$ in Eq. (38).

Consequently, the inclusive total cross section for multiple pion production σ_{tot} and the leading pion production cross section σ_ρ may be obtained by integrating these differential cross sections. We can also define the average central π^- multiplicity by

$$\langle n_{\pi^-}^c \rangle(\kappa) = \frac{\pi}{\sigma_{\text{tot}}} \int dp_\perp^2 \int dx \, h(s) f_c(x)$$

$$\times \frac{\exp[-p_\perp^2/\Lambda^2]}{\Lambda^2} \left[x^2 + \frac{1+2\kappa}{D^2} \right.$$

$$\left. \times \left(\frac{p_\perp^2}{m_N^2} + \varepsilon^2 \right) \right]^{-1/2}. \tag{40}$$

The integration range is determined by $p_\perp^2/(p_{\max}^*)^2 + x^2 \leq 1$. By evaluating this formula one can see that the multiplicity

$\langle n^c_{\pi^-}\rangle$ increases asymptotically logarithmically in s for $s \to \infty$. Applying charge conservation to the central pion distribution, making the above assumptions and in addition assuming π^+ and π^- distributions to be proportional to each other uniquely determines $d\sigma_6/dE'_{\pi^+}\equiv d\sigma_{\gamma p\to\pi^+ X}/dE'_{\pi^+}$. It is obtained by substituting

$$[1+(2/5)(1-\sigma_\rho/\sigma_{\text{tot}})/\langle n^c_{\pi^-}\rangle(\kappa)]f_c(x)+f_\rho(x)$$

for $f(x)$ in Eq. (38).

It is now straightforward to compute the fractions $r_c(\kappa)$ and $r_\rho(\kappa)$ of the incoming nucleon energy which go into the central and leading pions, respectively (see Appendix B). Figure 6 shows these fractions and the central and total π^- multiplicities as functions of s. Assuming a flat distribution for the outgoing nucleons, we then have

$$\frac{d\sigma_{p\to p}}{dE'_p}=\frac{\sigma_\rho}{2r_\rho(\kappa)E_p}\,\Theta\!\left[\frac{E'_p}{E_p}-1+2r_\rho(\kappa)\right]$$
$$+\frac{3}{5}\frac{\sigma_{\text{tot}}-\sigma_\rho}{2r_c(\kappa)E_p}\,\Theta\!\left[\frac{E'_p}{E_p}-1+2r_c(\kappa)\right],$$

$$\frac{d\sigma_{p\to n}}{dE'_n}=\frac{2}{5}\frac{\sigma_{\text{tot}}-\sigma_\rho}{2r_c(\kappa)E_p}\,\Theta\!\left[\frac{E'_n}{E_p}-1+2r_c(\kappa)\right]$$

$$(41)$$

for the charge retention and charge exchange cross sections, respectively. For the processes involving an incoming neutron, we assume that the cross sections are also given by the above expressions after substituting $p\leftrightarrow n$ and $\pi^+\leftrightarrow\pi^-$ everywhere. Figure 7 shows the differential cross sections for production of π^-, π^+, π^0, protons, and neutrons for an incoming proton for two different c.m. energies resulting from the formalism adopted above. Figure 8 shows the inclusive pion production cross sections for nucleons as a function of s. Figure 9 shows all the rates at redshift $z=0$ that affect the nucleons in the energy range we consider.

Pions produced by nucleons quickly decay to EM particles and neutrinos and feed the EM cascade. π^0 decays into photons ($\pi^0\to\gamma\gamma$), and $\pi^\pm$ decays to produce electrons, positrons, and neutrinos $[\pi^\pm\to\mu^\pm\nu_\mu(\bar\nu_\mu);\mu^\pm\to e^\pm\nu_e(\bar\nu_e)\bar\nu_\mu(\nu_\mu)]$ [89]. Since the decay time of pions is very short compared to the timescale in the problem, we assume that pions are converted into secondary particles instantaneously. The decay spectra of the secondary particles may be calculated easily [20]. The expressions for the decay spectra are given in Appendix C.

3. Neutron β-decay

Below $\sim 10^{20}$ eV, neutron β-decay is the fastest process among the interactions that affect nucleons in the problem. The neutron decay rate is $\Gamma=\Gamma_0/\gamma_n=1/\tau_n\gamma_n$, where τ_n is the neutron lifetime ($\tau_n\simeq 888.6\pm 3.5$ sec), and γ_n is the neutron Lorentz factor. The range R_n of a neutron is given as
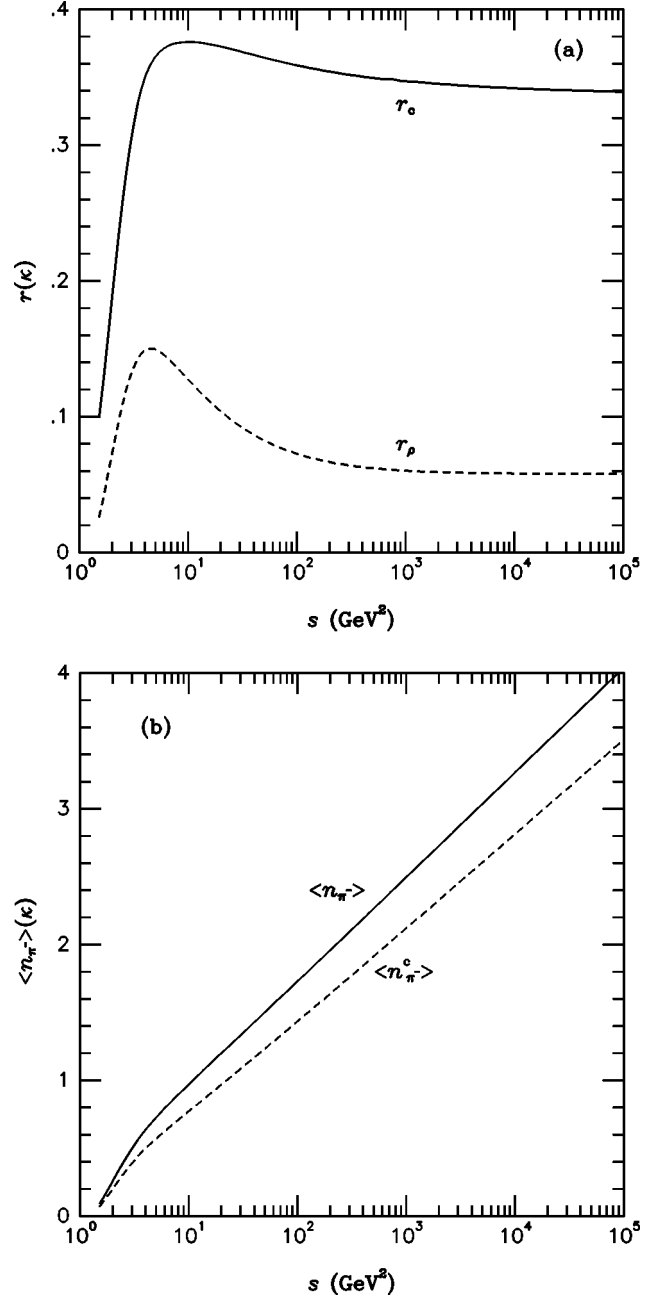

FIG. 6. (a) The fractions r_c and r_ρ of the incoming nucleon energy which goes into the central and leading pions, respectively, as functions of s; (b) The average central and total π^- multiplicities, $\langle n^c_{\pi^-}\rangle$ [see Eq. (40)] and $\langle n_{\pi^-}\rangle$ [resulting by substituting $f_c(x)\to f(x)$ in Eq. (40)] as functions of s.

$$R_n\simeq\frac{c}{\Gamma}=c\tau_n\gamma_n\simeq 0.9\!\left(\frac{E_n}{10^{20}\ \text{eV}}\right)\ \text{Mpc}. \qquad (42)$$

In calculating the spectrum of secondary particles, we neglect the proton kinetic energy in the neutron rest frame, as is usually done. The result can be found in standard textbooks such as Ref. [90].

Figure 10 shows the energy attenuation lengths for cascade photons and nucleons as functions of energy in the CEL approximation.
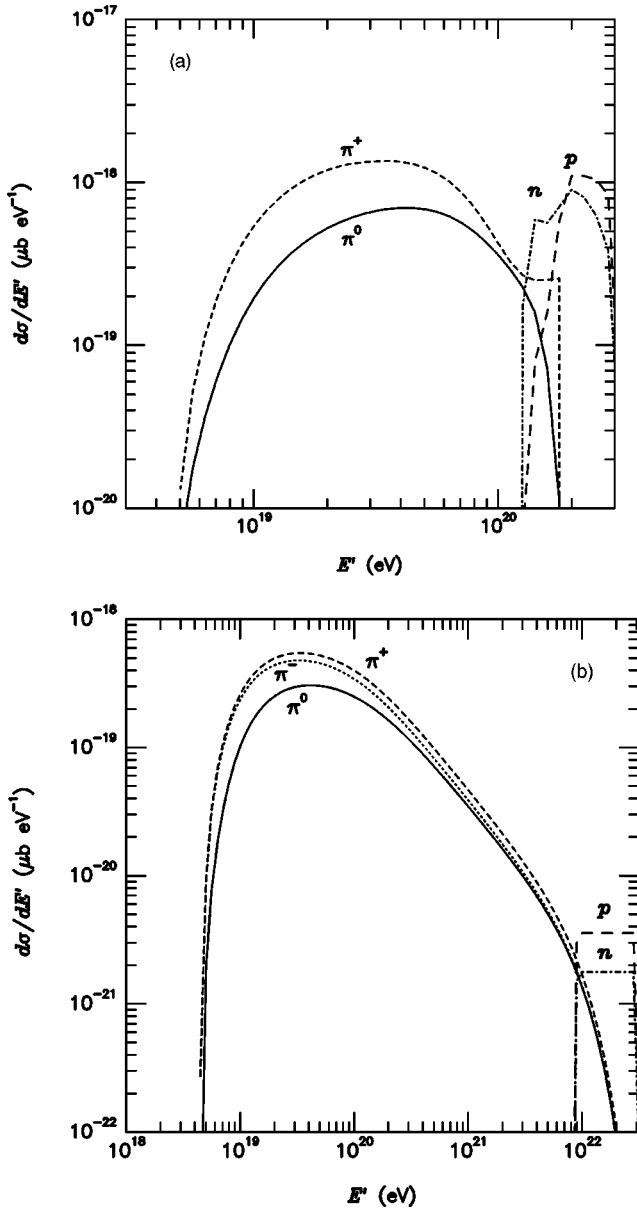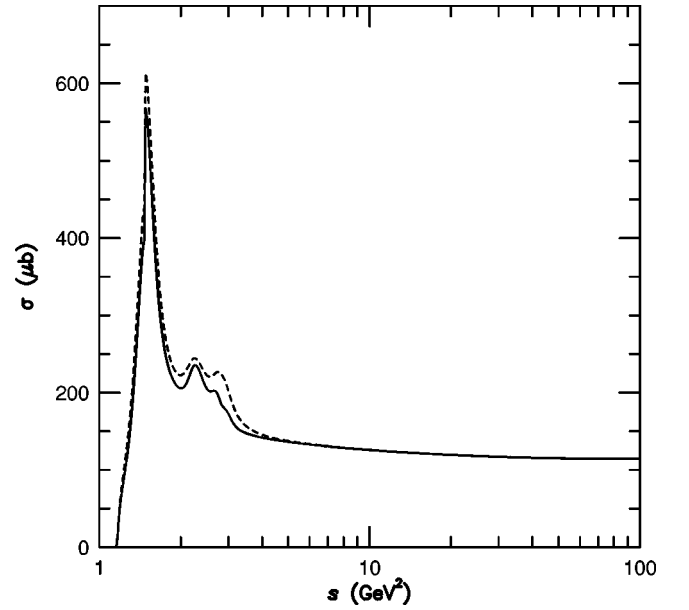
FIG. 8. The inclusive multiple pion production cross section for protons (solid line) and neutrons (dashed line) as a function of s.

$$N_a(E,z_i) = \frac{(1+z_i)^2}{r_i^2} F_a(E), \qquad (43)$$

where r_i is the comoving dimensionful source distance corresponding to redshift z_i ($r_i = 2H_0^{-1}[1-(1+z_i)^{-1/2}]$ in our cosmology), and solve the propagation equations for vanishing source terms. If we denote the resulting distribution at

FIG. 7. The differential cross sections for production of π^- (dotted lines), π^+ (short dashed lines), π^0 (solid lines), protons (long dashed lines), and neutrons (dash-dotted lines) for the collision of a proton of energy E with a background photon at squared CM energy s, from the formalism adopted in Sec. III B 2: (a) For $E=3\times10^{20}$ eV, $s=2.1$ GeV^2; (b) For $E=3\times10^{22}$ eV, $s=120$ GeV^2.

IV. COMPARISON WITH OTHER WORK

Before we apply the propagation code to specific HECR injection scenarios in the next section, we compare the predicted spectra with results from other investigations for some standard situations. For a discrete source producing a differential injection spectrum $F_a(E)$ of particle type a (in units of number per energy per time) at redshift $z=z_i$, we obtain the spectrum $j_a(E)$ (in units of number per area per time per solid angle per energy) observed at $z=0$ in the following way: we impose the boundary condition
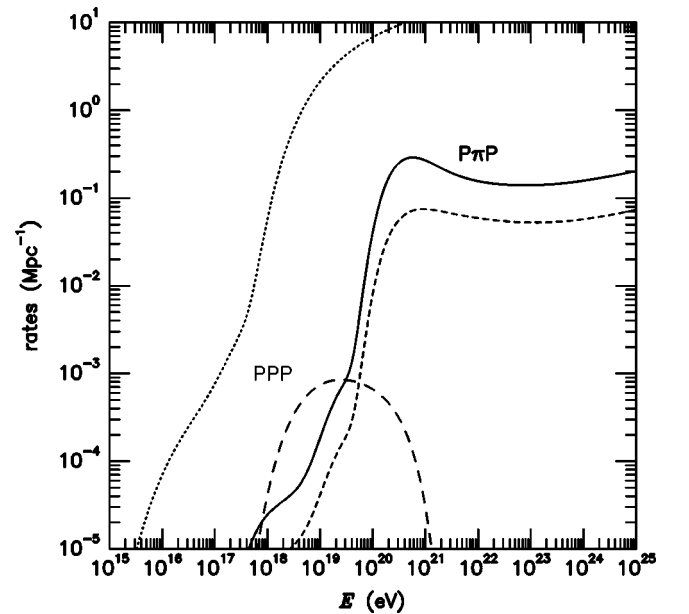

FIG. 9. The interaction rates and energy attenuation rates for multiple pion production (solid line and short dashed line, respectively) and PPP (dotted line and long dashed line, respectively). The rates were obtained by folding the cross sections and inelasticity weighted cross sections with the present background photon spectrum shown in Fig. 2.
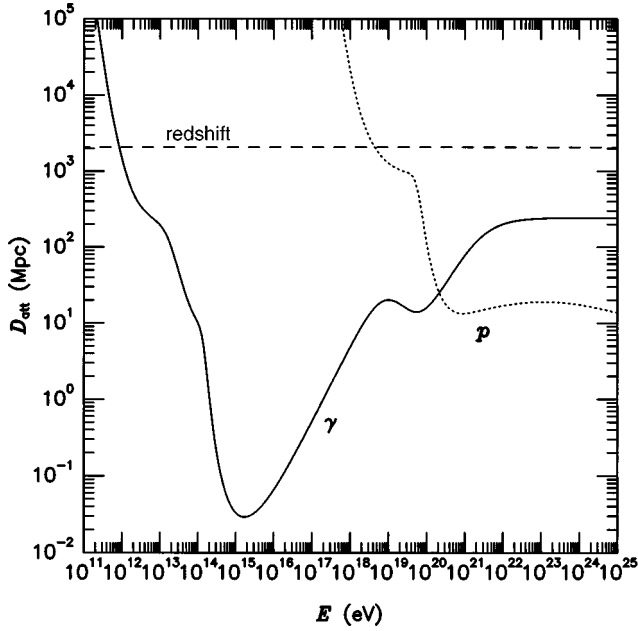
FIG. 10. The energy attenuation lengths for cascade photons and for protons as a function of energy assuming the radiation background photon spectrum shown in Fig. 2. These curves were obtained by running the code over small distances and ignoring the production of non-leading particles, which corresponds to the CEL approximation.

$z=0$ by $N_a(E)$, then $j_a(E)=N_a(E)/(4\pi)$ and the modification factor $M_a(E,z_i)$, defined as in Ref. [43,45], is given by

$$M_a(E,z_i) \equiv \frac{4\pi d_L^2 j_a(E)}{F_a(E)} = (1+z_i)^4 \frac{N_a(E)}{N_a(E,z_i)}, \quad (44)$$

where we used the luminosity distance $d_L \equiv r_i(1+z_i)$ [91].

In Fig. 11 we plot the modification factors as defined in Ref. [45] for discrete sources injecting protons with a power law at a given distance along with the corresponding curves from Ref. [52]. It can be seen that our results lie somewhat between results from Refs. [52] and [48]. In Fig. 12 we compare the nucleon, γ-ray and neutrino fluxes computed for monoenergetic proton injection at a given distance with results from Ref. [52]. In our prediction the secondary γ-ray flux at the low energy side is higher than the one given in Ref. [52] by a factor $\simeq 10$. We attribute this difference to the fact that the differential multiple pion production cross section used in our analysis (see Fig. 7) peaks at low energies. In Fig. 13 we consider the case of power law injection by a single source and compare the nucleon and γ-ray fluxes with corresponding results in Ref. [48]. The nucleon fluxes agree well, whereas, again, our prediction for the γ-ray flux is higher at the low energy side and lower at the high energy side. Since Refs. [48,52] do not give detailed information on their treatment of pion production, it is hard to give an exhaustive explanation of these differences. This, however, will not have an influence on our considerations where secondary γ-ray production by nucleons plays a minor role.

V. APPLICATION TO MODELS OF HECR ORIGIN

We are now in a position to compute the cosmic and γ-ray fluxes predicted by various models of HECR origin. Since there is currently no unambiguous information on HECR composition, we will normalize the predicted sum of γ-ray and nucleon fluxes to the observed HECR flux. This is done to optimally enable an explanation for the events above 10^{20} eV without overshooting the UHE flux at lower energies (which may be explained by more conventional components) or predicting an excessive integral flux above 10^{20} eV. We estimate the uncertainty in the predicted γ-ray flux at lower energies induced by this normalization procedure to be less than a factor $\simeq 3$.

A. GUT scale physics models

As already mentioned in the Introduction, it has been suggested that HECRs may have a nonacceleration origin [27–34] such as the decay of supermassive elementary ''X'' particles associated with grand unified theories (GUTs), for example. These particles could be radiated from topological defects (TDs) formed in the early universe during phase transitions caused by spontaneous breaking of symmetries implemented in these GUTs (for a review on TDs, see [92]). This is because TDs, such as ordinary and superconducting cosmic strings, domain walls and magnetic monopoles, are topologically stable but nevertheless can release part of their energy in the form of these X particles due to physical processes like collapse or annihilation. The corresponding injection rate of X particles dn_X/dt as a function of cosmic time t is usually parametrized as

$$\frac{dn_X}{dt} \propto t^{-4+p}, \quad (45)$$

where $p \geq 0$ depends on the evolution of TDs. For example, X particle release from a network of ordinary cosmic strings in the scaling regime would correspond to $p=1$ if one assumes that a constant fraction of the total energy in closed loops goes into X particles [29,31]. Annihilation of magnetic monopoles and antimonopoles [27,33] predicts $p=1$ in the matter dominated and $p=3/2$ in the radiation dominated era [58] whereas the simplest models for superconducting cosmic strings lead to $p=0$ [28]. A constant comoving injection rate corresponds to $p=2$ and $p=5/2$ during the matter and radiation dominated era, respectively.

The X particles with typical GUT scale masses m_X of the order of 10^{16} GeV subsequently decay into leptons and quarks. The strongly interacting quarks fragment into a jet of hadrons which results in mesons and baryons that are typically of the order of 10^4–10^5. It is assumed that these hadrons then give rise to a substantial fraction of the HECR flux as well as a considerable neutrino flux. The shapes of the nucleon and γ-ray spectra predicted within such TD models are thus expected to be universal (i.e., independent of the specific process involving any specific kind of TD) at ultrahigh energies and to be dependent only on the physics of X particle decay. This is because at HECR energies nucleons and γ-rays have attenuation lengths in the cosmic microwave
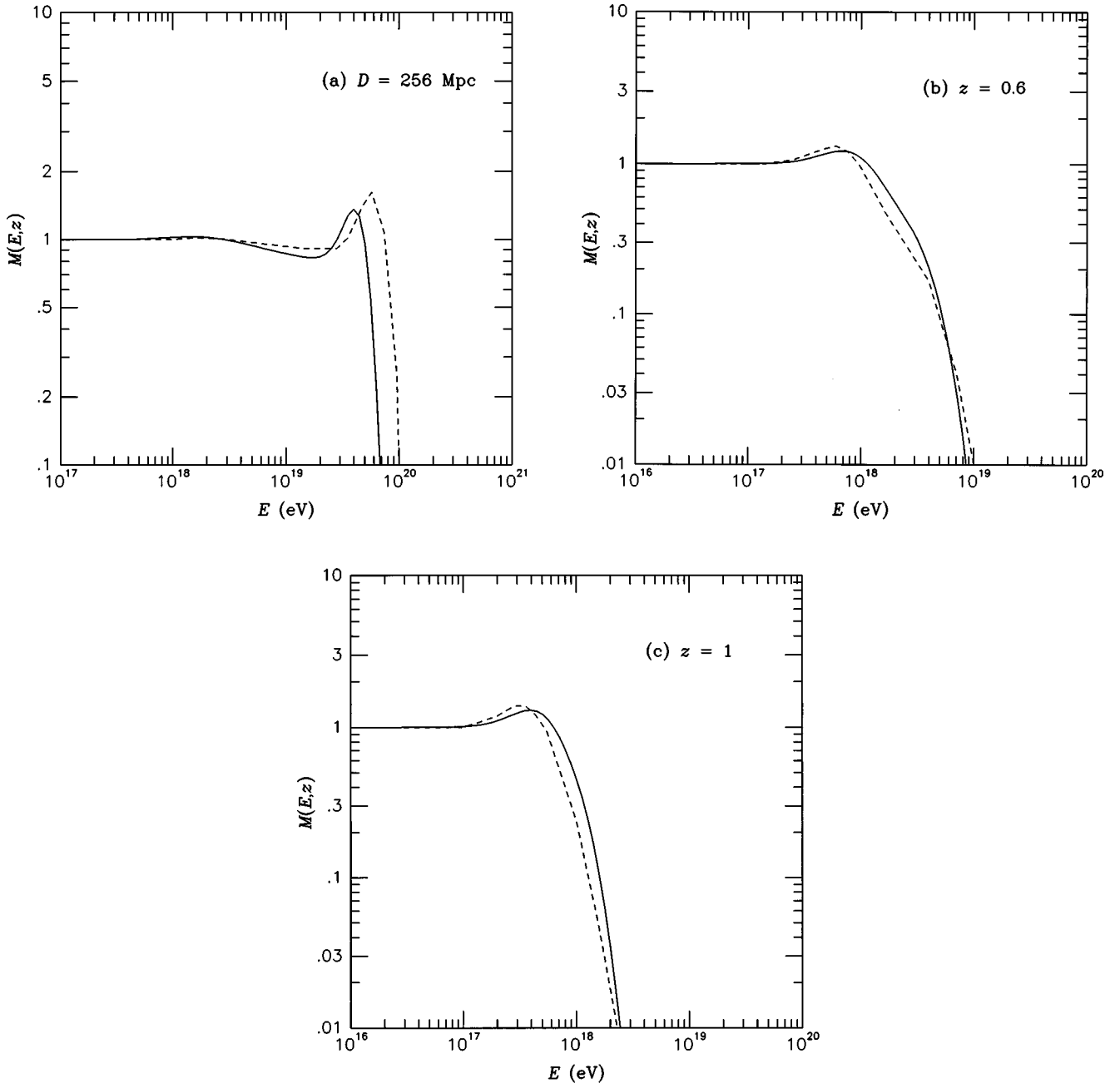
FIG. 11. The modification factors as defined in Ref. [45] for discrete sources injecting a E^{-2} proton spectrum extending up to 3×10^{20} eV at a given distance d or redshift z resulting from our analysis (solid lines). Also shown are the corresponding curves from Protheroe and Johnson [52] (dashed lines): (a) For $d = 256$ Mpc; (b) For $z = 0.6$; (c) For $z = 1$. For further comparison with results from Refs. [45,48] see the discussion in Ref. [52].

background (CMB) which are small compared to the Hubble scale. Cosmological evolutionary effects which depend on the specific TD model and are usually parametrized by Eq. (45) are therefore negligible. In contrast, the predicted neutrino flux and the γ-ray flux below the pair production threshold on the CMB [see Eq. (1)] depend on the energy release integrated over redshift and thus on the specific TD model.

We now discuss the particular form of the particle injection spectra expected from X particle release. We assume that each X-particle decays into a lepton and a quark each of

an energy approximately half of the X particle mass m_X. For reasonable extragalactic field strengths, the lepton (which we assume to be an electron in the following) will quickly be degraded by synchrotron loss producing synchrotron photons of a typical energy given by Eq. (8). This energy is typically much smaller than 10^{20} eV where the resulting contribution to the γ-ray flux is likely to be buried below the charged CR flux. For that reason, the GUT-scale lepton was usually omitted. However, for high EGMF strengths the synchrotron peak can approach 10^{20} eV and thus could become relevant. For the present analysis we thus include the source term for
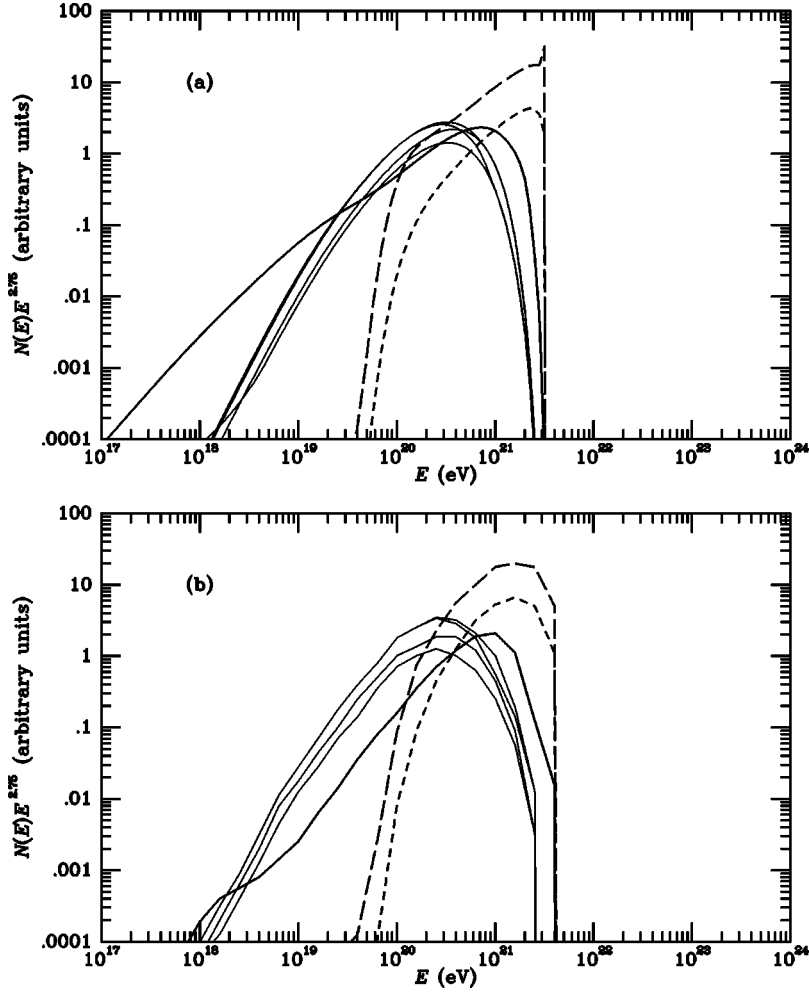
FIG. 12. The differential fluxes of γ-rays (solid line), protons (long dashed line), neutrons (short dashed line) and ν_μ, $\bar{\nu}_\mu$, ν_e, $\bar{\nu}_e$ (thin solid lines in decreasing order) for monoenergetic proton injection at an energy $E=10^{21.5}$ eV and a distance $d=32$ Mpc: (a) Result from our analysis in arbitrary units; (b) Corresponding results from Ref. [52].

the GUT-scale lepton by writing its injection flux at energy E and time t as

$$\Phi_e(E,t) = \frac{dn_X(t)}{dt}\,\delta(E-m_X/2),\qquad(46)$$

in units of particles per volume per time per energy.

The quark from X particle decay hadronizes by jet fragmentation and produces nucleons, γ-rays and neutrinos, the latter two from the decay of neutral and charged pions in the hadronic jets. The hadronic route is expected to produce the largest number of particles. The resulting effective injection spectrum for particle species a from the hadronic channel can be written as

$$\Phi_a(E,t) = \frac{dn_X(t)}{dt}\,\frac{2}{m_X}\,\frac{dN_a(x)}{dx},\qquad(47)$$

where $x\equiv 2E/m_X$, and dN_a/dx is the effective fragmentation function describing the production of the particles of species a from the original quark.

The spectra of the hadrons in a jet produced by the quark are, in principle, given by quantum chromodynamics (QCD). Suitably parametrized QCD motivated hadronic spectra that fit well the data in collider experiments in the GeV–TeV energies have been suggested in the literature [27]. In this paper, the *total* hadronic fragmentation spectrum dN_h/dx is taken to be of the form [27]

$$\frac{dN_h(x)}{dx} = \begin{cases} \dfrac{15}{16}x^{-1.5}(1-x)^2 & \text{if } x_0 \leq x \leq 1, \\ 0 & \text{otherwise,} \end{cases}\qquad(48)$$

where the lower cutoff x_0 is typically taken to correspond to a cutoff energy ~ 1 GeV. The spectrum Eq. (48) obeys energy conservation, $\int_{x_0}^1 dx\,x(dN_h(x)/dx)=1$. This function is a good working model for a fragmentation spectrum. It also enables us to compare with other work (e.g. Ref [53]). Assuming a nucleon content of $\simeq 3\%$ and the rest equally distributed among the three types of pions, we can write the fragmentation spectra as [32,51]
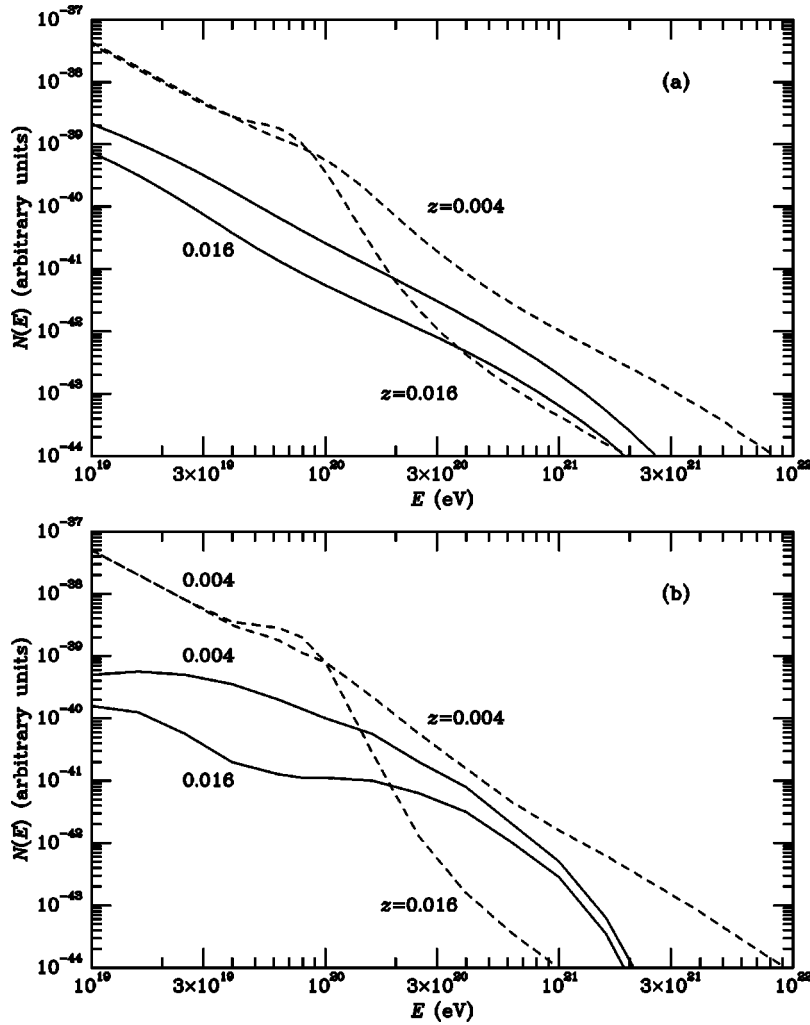
FIG. 13. The differential fluxes of γ-rays (solid lines) and nucleons (long dashed lines) from a discrete source injecting a E^{-2} proton spectrum extending up to 10^{22} eV, located at the redshift indicated: (a) Result from our analysis in arbitrary units; (b) Corresponding results from Ref. [48].

$$\frac{dN_N(x)}{dx} = (0.03) \frac{dN_h(x)}{dx},$$

$$\frac{dN_{\pi^+}}{dx} = \frac{dN_{\pi^-}}{dx} = \frac{dN_{\pi^0}}{dx}$$

$$= \left(\frac{0.97}{3}\right) \frac{dN_h(x)}{dx}. \tag{49}$$

From the pion injection spectra one gets the resulting contribution to the injection spectra for γ-rays, electrons and neutrinos by applying the formulas in Appendix C.

Independent of the spectral shapes of the predicted nucleon and γ-ray fluxes, the question for the absolute normalization of the injection rates dn_X/dt in Eqs. (45), (46) and (47) arises. It has been shown, for example for cosmic strings [29,31] and annihilation of magnetic monopoles and antimonopoles [33], that at least some TD models are capable of producing an observable HECR flux if reasonable parameters are adopted. For the purposes of this paper we

will therefore not consider this issue and simply adopt the normalization procedure mentioned above.

TD models of HECR origin are subject to a variety of constraints mostly of cosmological nature. These are mainly due to the comparatively substantial predicted energy injection at high redshift [see Eq. (45)]. Note that more conventional CR sources like galaxies start to inject energy only at a redshift of a few. Using an analytical approximation for the cascade spectrum below the pair production threshold on the CMB resulting from X particle injection, one can derive constraints from cascading nucleosynthesis and light element abundances, CMB distortions, and the measured γ-ray background [61,60,62] in the 100 MeV region [58], as well as from observational limits on the γ-ray to charged CR flux ratio between 10^{13} eV and 10^{14} eV [93,34]. The 100 MeV γ-ray background constraint was first discussed in Refs. [50, 57]. In the context of top-down models it was applied in Refs. [94, 95] on the basis of analytical approximations.

In an accompanying letter [96], we obtain the constraints due to this 100 MeV diffuse γ-ray flux applied to various cases of more realistic UHE CR models, and discuss the

implications in great detail. Here we concentrate on the generic features of the propagated spectrum that arises from a typical TD model.

Recently, there has been a claim [52] that TD models may be ruled out altogether due to overproduction of γ-rays in the range between the knee and $\sim 10^{19}$ eV. This would occur for EGMFs stronger than about 10^{-10} G due to synchrotron radiation from the electronic component of the TD induced flux which was normalized to the observed flux at 3×10^{20} eV. However, in my opinion, the argument in Ref. [52] suffers from several shortcomings: first, monoenergetic injection of protons and γ-rays was used instead of the more realistic injection spectra such as the one discussed above in Eqs. (48) and (49). And second, only the case of a single, discrete TD source at a fixed distance from the observer was considered instead of more realistic source distributions and evolution histories. Finally, electron deflection due to the EGMF which can influence the processed spectrum from a single source was neglected. Nevertheless, I simulated the situation of Fig. 13 in Ref. [52] for an EGMF of 10^{-9} G on which their claim is based. As a result I got a spectrum whose shape is roughly similar to Fig. 13 in Ref. [52], but the details of the spectrum differed somewhat, part of which can be attributed to a different model of the radiation background. The synchrotron peak I got was about an order of magnitude lower than in Ref. [52] relative to other parts of the spectrum. Most importantly, however, we observe that if the spectrum is normalized to the highest energy event this model would predict simply too many events above 10^{20} eV including the original injection peak. Therefore, the model adopted in Ref. [52] is not a realistic model for UHE CRs to start with. I thus conclude that it is not possible to rule out TD models on the basis of the discussion in Ref. [52].

The redshift range of energy injection contributing to the γ-ray flux at energy E_γ today is given by $1+z \lesssim [E_{th}(z=0)/E_\gamma]^{1/2}$ where $E_{th}(z=0)$ is the PP threshold on the CMB at $z=0$ [see Eq. (1)]. Since our interest is in the γ-ray flux at $E_\gamma \gtrsim 100$ MeV, we integrate up to $1+z_{max}=10^3$. The spectrum in this energy range converges well before we reach this redshift. A word of caution is in order for the predicted neutrino spectra. The UHE neutrinos interact with the universal neutrino background with $T_\nu \sim 1.95$ K, and produce $l\bar{l}$ where $l=e,\mu,\tau,\nu,q,\dots$ via Z_0 resonance [32,41]. The decay products of μ,τ,q contain secondary neutrinos. Here we consider only simple absorption of UHE neutrinos, i.e. we integrate up to the average absorption redshift z_{abs} due to this interaction [32]. The neutrino spectra also converge rather fast with increasing redshift for the parameters we used for TD models. Furthermore, the modification to the neutrino spectra due to the cascading by the aforementioned interaction is expected to be small for these parameters [41]. Therefore, the neutrino spectra given in this paper are expected to be good approximations to the real converged spectra. We leave a more detailed discussion of the UHE neutrinos to another paper [97].

We performed simulations assuming uniform injection rates given by Eqs. (46)–(49) for $m_X = 2 \times 10^{25}$ eV and an injection history given by Eq. (45) for $p=1$ (representative
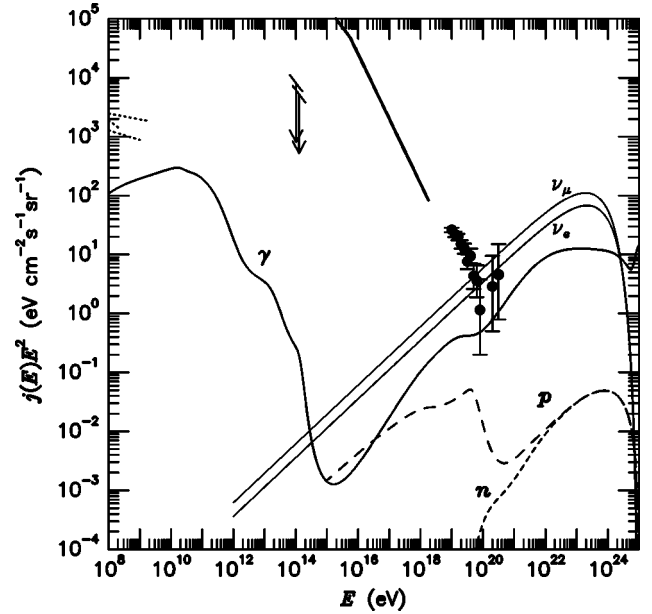

FIG. 14. Predictions for the differential fluxes of γ-rays (solid line), protons (long dashed line), neutrons (short dashed line), and $\nu_\mu(\bar{\nu}_\mu), \nu_e(\bar{\nu}_e)$ (thin solid lines in decreasing order) by a typical topological defect scenario for a vanishing EGMF. This model assumes uniform injection rates with spectra given by Eq. (46) and (47) for the QCD motivated fragmentation functions Eq. (48) and (49) for $m_X = 2 \times 10^{25}$ eV. The injection history is given by Eq. (45) for $p=1$. Also shown are the combined data from the Fly's Eye [8,9] and the AGASA [11,12] experiments above 10^{19} eV (dots with error bars), piecewise power law fits to the charged CR flux (thick solid line) and observational upper limits on the γ-ray flux around 100 MeV from Refs. [60–62] (dotted lines in decreasing order). The arrows indicate the limits on the γ-ray to charged CR flux ratio from Ref. [93].

of scenarios based on ordinary cosmic strings and monopole-antimonopole annihilation). Figure 14 shows the results for a negligible EGMF and assuming our IR-O background model. The result without the IR-O background and that by the CEL approximation are shown in Fig. 15. First, note that for a vanishing EGMF the γ-ray flux dominates the nucleon flux at UHEs within this model, and is higher by more than an order of magnitude compared with the predictions within the CEL approximation even at around 10^{20} eV. This is due to the influence of non-leading particles (lower energy particles in interactions) on the development of the EM cascade. The ''plateau'' at around 10^{19} eV is due to a small pile-up of energy below the threshold of pair production on the universal radio background. The big dip centered at about 10^{15} eV is due to the absorption peak by pair production on the CMB. The γ-ray flux level between $\sim 10^{11}$ eV and $\sim 10^{14}$ eV is depleted somewhat due to the IR-O background. In the extreme case of absence of any IR-O flux, the γ-ray flux at that energy increases by a factor of about 100 relative to the level predicted by our IR-O background model, whereas the flux below $\simeq 10$ GeV decreases by a factor of about 10 for a vanishing IR-O flux (see Fig. 15). On the other hand, the neutrino flux is typically at least one order of magnitude larger than the other components at UHE. However, we note
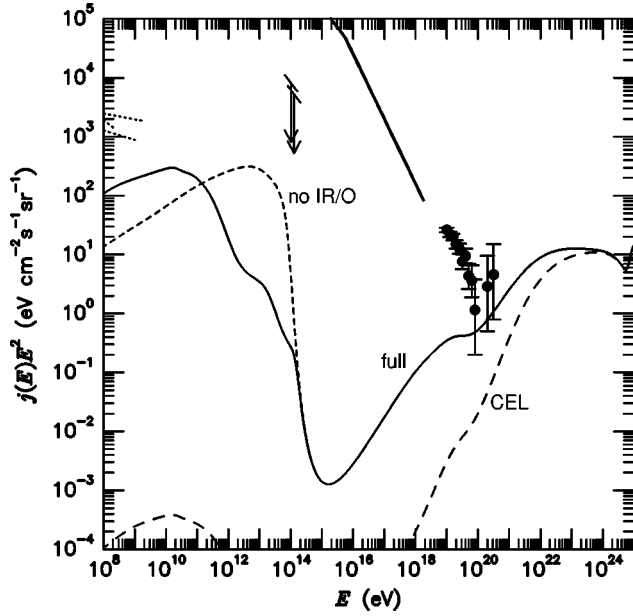
FIG. 15. Comparison of the γ-ray flux for the full numerical simulation (solid, same as Fig. 14) with the prediction by the CEL approximation in which non-leading particles in the EM cascade are neglected (long dashed line) and with the result assuming no IR-O background (short dashed line).

that the probability that these UHE neutrinos generate a shower in the atmosphere is smaller than 10^{-5} [17].

In Fig. 16, we show cases with non-negligible EGMFs. For an EGMF strength $\gtrsim 10^{-11}$ G, the γ-ray flux in the synchrotron dominated energy regime is determined by photon absorption rather than cascading and thus the spectrum becomes harder. At the same time, a synchrotron radiation peak appears at a lower energy. Whereas the synchrotron radiation peak energy increases with the EGMF strength [Eq. (8)], the critical energy above which the synchrotron loss dominates over inverse Compton scattering decreases with the EGMF strength. Therefore, the propagated spectrum shows a nontrivial dependence on the EGMF strength. Nonetheless, after a proper normalization the γ-ray flux at around 100 MeV tends to get bigger by a factor of a few compared to the case with a negligible EGMF.

B. Gamma ray burst models

Recently, it has been suggested that UHE CR could be associated with cosmological GRBs [24–26]. This was mainly motivated by an apparent numerical coincidence: Assuming that each (cosmological) GRB releases an amount of energy in the form of UHE CRs which is comparable to the total γ-ray output normalized to the observed GRB rate (about 10^{51} erg per burst), the predicted and the observed UHE CR flux at the Earth are comparable. It should be mentioned, however, that it is not clear whether constraints on cosmological GRB distributions are consistent with HECR observations [98].

In these models protons are accelerated to UHE via first order Fermi acceleration. Since there are no firm predictions for the injection spectrum, I assume the hardest possible
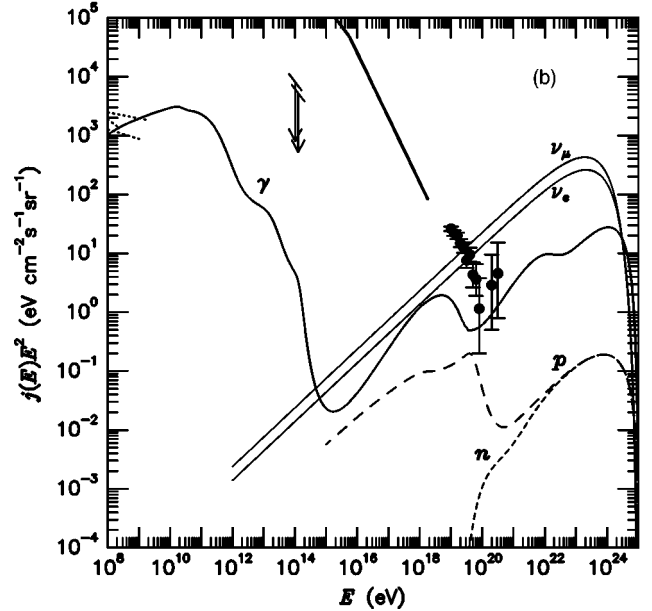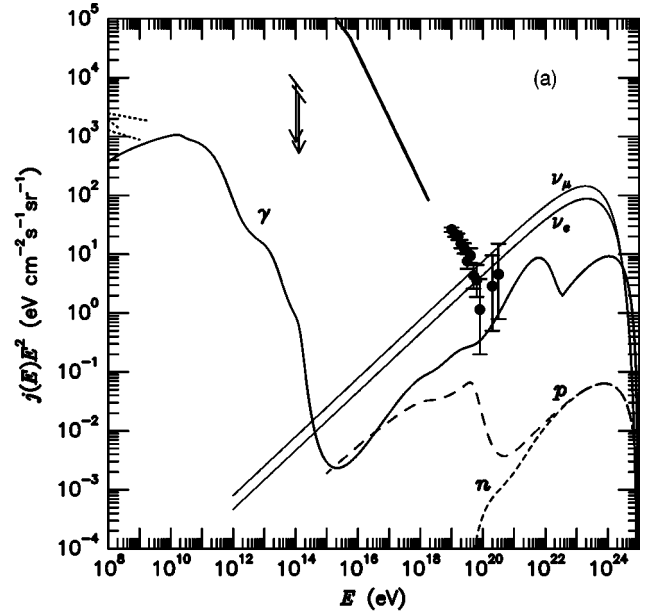

FIG. 16. (a) Same as Fig. 14, but for an EGMF of 10^{-9} G; (b) Same as Fig. 14, but for an EGMF of 10^{-12} G.

spectrum proportional to E^{-2} up to a maximal energy of 10^{23} eV. Furthermore, assuming a constant comoving injection rate up to some maximal redshift z_{max}, we can write

$$\Phi_p(E,t) \propto t^{-2} E^{-2} \Theta(z_{max} - z) \Theta(10^{23} \text{ eV} - E). \quad (50)$$

The authors of Ref. [26] pointed out that bursting sources in combination with deflection of protons in the EGMF could lead to UHE CR spectra with a time variability on a scale of ~ 50 yr. This may allow reasonable fits to the observed HECR spectrum. However, we only consider the continuous injection of CRs in this paper for illustrative purposes. Since the γ-ray background depends only on the average flux, the only uncertainty in its flux level comes from the fit to the HECR events. I estimate the uncertainty introduced by nor-
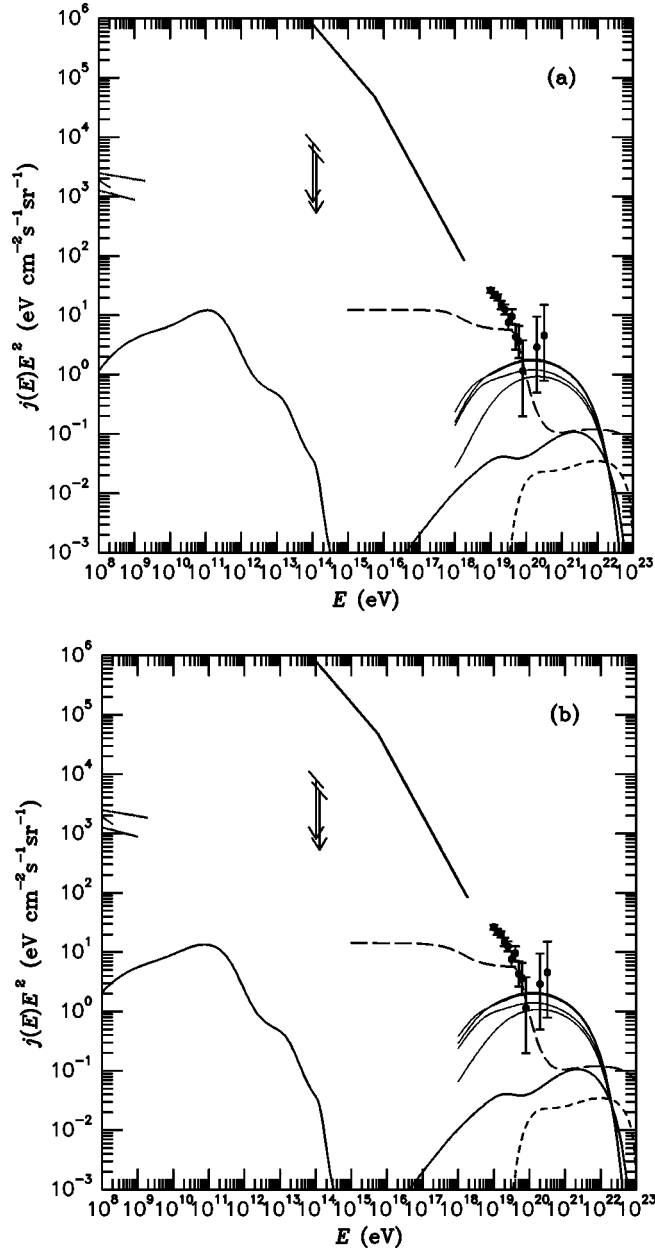
VI. CONCLUSIONS

I have performed detailed numerical simulations for the propagation of extragalactic nucleons, γ-rays, and electrons in the energy range between 10^8 eV and 10^{25} eV. We have explored various features in the propagated spectra which arise from generic models which associate HECRs with GUT scale physics or with cosmological GRBs. These models may be constrained by observational data such as the diffuse γ-ray background at 100 MeV region, and the limits on the γ to charged CR flux ratio at or below 100 TeV, as well as the UHE CR flux itself.

The CEL approximation usually does not take the IR-O background into account, and thus may not be directly compared to the numerical calculation because the presence of the IR-O background may affect the γ-ray flux level at 100 MeV by an order of magnitude. There is also a significant difference for the UHE spectrum between predictions by the CEL approximation and our numerical simulation. For a negligible EGMF, the EM cascading effect is quite important throughout the whole energy range in determining the propagated spectrum in the case of the TD models. On the other hand, an EGMF stronger than $\sim 10^{-11}$ G stops the cascade at UHEs and the UHE end of the spectrum is suppressed significantly. The level of the γ-ray flux at about 100 MeV is relatively higher as a result. However, these results are rather insensitive to different models of the IR-O background [64], although they are somewhat dependent on the poorly known universal radio background flux.

We stress that this numerical code is very general in its nature. For any given model with the specified injection history and the source distribution, one can obtain an accurate propagated spectrum of various particle species, and constrain the model with observational data. With the arrival of the anticipated Pierre Auger Cosmic Ray Observatories [59], it is expected that the UHE end of the CR spectrum will be known with much better accuracy. Constraints derived from the influence of CR propagation on the observed spectrum will then be one of the most powerful tools in discriminating between models of HECR origin.

FIG. 17. Predictions for the differential fluxes of γ-rays (solid line), protons (long dashed line), neutrons (short dashed line), and ν_μ, $\bar{\nu}_\mu$, ν_e, $\bar{\nu}_e$ (thin solid lines from the top) by the GRB injection scenario given by Eq. (50) for vanishing EGMF for: (a) $z_{max}=1$; (b) $z_{max}=4$. Observational data and constraints are presented as in Fig. 14.

malizing the average flux to be less than a factor 1.5. Figure 17 shows the results for various values of z_{max}. The γ-ray flux at 100 MeV in this case usually falls much below the level for a TD model because the γ-rays in the case of this GRB model are secondaries produced from photopion production during the propagation of the primary nucleons. Therefore, these models are currently unconstrained by the γ-ray background constraint. We also note that this conclusion is insensitive to the initial redshift at which the sources began injecting particles [compare Figs. 17(a),(b)].

APPENDIX A: TRIPLET PAIR PRODUCTION

The expressions for the differential spectra of produced pairs and the recoiling electron (positron) for TPP by a very

energetic electron on a soft photon can be found in many papers [76–78]. I adopt the analytic approach used in [77]. For an interaction of an electron of energy E with a photon of energy ϵ ($E \gg \epsilon$), the double differential cross section with respect to the positron produced with energy E_+ at solid angle Ω_+ can be expressed as

$$\frac{d^2\sigma}{dE_+ d\Omega_{p_+}} = \sigma_T \cdot \frac{3\alpha}{16\pi^3} \frac{p_+}{p \cdot k} \frac{(\rho_t^2 - 4)^{1/2}}{\rho_t}$$

$$\times \int A_t d\Omega_{p'}, \quad (A1)$$

where $p \cdot k$ is the scalar product of the initial electron and photon four-momenta, p_+ is the magnitude of the produced positron three-momentum, $\Omega_{p'}$ is the solid angle of the recoiling electron, and ρ_t and A_t are given in Ref. [77]. The single differential cross section with respect to the positron energy may be obtained by integrating Eq. (A1) over the

positron solid angle Ω_+ numerically. The differential cross section for the produced electron is identical to that for the positron due to symmetry. In doing the integration, it is useful to use the approximation where the dependence of the cross section on the azimuthal angle of the outgoing particles in the cosmic ray frame is neglected, as was mentioned before.

Finally, we can obtain the total TPP cross section by integrating Eq. (A1) numerically over the kinematic range of electron and positron energies given by

$$E_{\max,\min} = \frac{E_{\text{tot}}(s_0 - m_e^2) \pm P_{\text{tot}}[s_0(s_0 - 4m_e^2)]^{1/2}}{2s_0 + m_e^2}, \quad (A2)$$

where $s_0 \equiv \epsilon(E+p)$, and E_{tot} and P_{tot} are the total incident energy and momentum, respectively.

I also give here the kinematic energy range for the outgoing electron and positron and the recoiling proton in case of pair production by protons (Sec. III B 1):

$$E_{\max,\min} = \frac{E_{\text{tot}}(s_0 - m_e\lambda) \pm P_{\text{tot}}[s_0^2 - 2m_e s_0(m_e + \lambda) + m_e^2(m_e^2 - m_N^2)/2]^{1/2}}{2s_0 + m_N^2}, \quad (A3)$$

where s_0 is as defined previously, $\lambda \equiv [(m_e^2 + m_N^2)/2]^{1/2}$.

APPENDIX B: PHOTOPION PRODUCTION

First, we express the differential cross sections for single pion production in terms of the CRF energies E'_a, where $a = N, \pi$:

$$\frac{d\sigma_i}{dE'_N}, \frac{d\sigma_i}{dE'_\pi} = \frac{2\pi}{E_N} \frac{1 + 2\kappa}{D} \sum_{j=0}^{K} a_{ij}(\kappa)(x^*)^j \begin{cases} 1 & \text{for } i=1 \text{ (charge retention)} \\ (1 - \beta^* x^*)^{-1/2} & \text{for } i=2,3 \text{ (charge exchange)} \end{cases} \quad (B1)$$

where $\beta^* = D/(\kappa + \varepsilon^2/2)$ and x^* can be expressed as a function of E'_N or E'_π and E_N:

$$x^* = \frac{(1 + 2\kappa)(E'_N/E_N) - 1 - \kappa - \varepsilon^2/2}{D} = -\frac{(1 + 2\kappa)(E'_\pi/E_N) - \kappa - \varepsilon^2/2}{D}. \quad (B2)$$

Finally, we compute the fractions $r_c(\kappa)$ and $r_\rho(\kappa)$ of the incoming nucleon energy going into the central and leading pions. These fractions are given by integrating the differential cross section $d\sigma/dE_\pi$ for the respective process, weighted by the pion energy E_π, in the CRF, and dividing by the corresponding total cross section. Using Eq. (35),

$$E_\pi = \frac{E_N}{m_N} \frac{E_\pi^* - p_\parallel^*}{(1 + 2\kappa)^{1/2}} = \frac{E_N}{m_N} \frac{p_{\max}^*}{(1 + 2\kappa)^{1/2}} \left[\left(x^2 + \frac{p_\perp^2 + m_\pi^2}{(p_{\max}^*)^2} \right)^{1/2} - x \right], \quad (B3)$$

and Eq. (34), we end up with

$$r_\rho(\kappa) = \frac{\pi}{\sigma_\rho} \frac{D}{1 + 2\kappa} \int dp_\perp^2 \int dx 2h(s) f_\rho(x) \frac{\exp[-p_\perp^2/\Lambda^2]}{\Lambda^2} \left\{ 1 - x \left[x^2 + \frac{1 + 2\kappa}{D^2} \left(\frac{p_\perp^2}{m_N^2} + \varepsilon^2 \right) \right]^{-1/2} \right\}. \quad (B4)$$

Again, the integration ranges are obtained by the requirement $p_\perp^2/(p_{\max}^*)^2 + x^2 \leq 1$. The formula for $r_c(\kappa)$ can be obtained from this by substituting $\sigma_\rho \to \sigma_{\text{tot}} - \sigma_\rho$ and $2f_\rho(x) \to [3 + (2/5)(1 - \sigma_\rho/\sigma_{\text{tot}})/\langle n_{\pi^-}^c\rangle(\kappa)] f_c(x)$, where $\langle n_{\pi^-}^c\rangle(\kappa)$ was given in Eq. (40).

APPENDIX C: PION DECAY SPECTRA

First, we define the decay spectrum $N_a(E)$ as the differential number of the secondary particle a at energy E. Then the spectrum is normalized as

$$\int dE N_a(E) = n_a, \tag{C1}$$

where n_a is the number of particles a produced by decay of a single pion. For example, $n_\gamma = 2$ for π^0 decay.

First, the photon spectrum from π^0 decay is

$$N_\gamma(E) = \frac{2}{E_\pi} \quad \text{for } E \leq E_\pi. \tag{C2}$$

Before we calculate the charged pion decay spectra, we note the fact that the pions produced from photopion production are always relativistic. Thus, we may make the relativistic approximation for both pions and the resulting muons. For example, the decay spectra of π^+ read:

$$N_{e^+}(E) = N_{\bar{\nu}_\mu}(E) \simeq \begin{cases} \dfrac{1}{(1-r)E_\pi}(A_0 + A_2 z^2 + A_3 z^3) & \text{for } E \leq rE_\pi \\[2mm] \dfrac{1}{(1-r)E_\pi}(B_0 + B_0' \ln z + B_2 z^2 + B_3 z^3) & \text{for } rE_\pi \lesssim E \leq E_\pi, \end{cases}$$

$$N_{\nu_\mu}(E) = \frac{1}{(1-r)E_\pi} \quad \text{for } E \leq (1-r)E_\pi$$

$$N_{\nu_e}(E) \simeq \begin{cases} \dfrac{1}{(1-r)E_\pi}(C_0 + C_2 z^2 + C_3 z^3) & \text{for } E \leq rE_\pi \\[2mm] \dfrac{1}{(1-r)E_\pi}(D_0 + D_0' \ln z + D_1 z + D_2 z^2 + D_3 z^3) & \text{for } rE_\pi \leq E \leq E_\pi, \end{cases} \tag{C3}$$

where $r \equiv m_\mu^2/m_\pi^2$, $z \equiv E/E_\pi$, and coefficients are given as

$$(A_0, A_2, A_3) = (0.94486, -2.7892, 1.2397),$$

$$(B_0, B_0', B_2, B_3) = (-2.4126, -2.8951, 4.3426, -1.9300),$$

$$(C_0, C_2, C_3) = (1.1053, -4.46883, 3.71887),$$

and

$$(D_0, D_0', D_1, D_2, D_3) = (13.846, 5.37053, -28.1116, 20.0558, -5.7902).$$

The average energies of the secondary particles are $\langle E_{e^+}\rangle = \langle E_{\bar{\nu}_\mu}\rangle = 0.265 E_\pi$, $\langle E_{\nu_e}\rangle = 0.257 E_\pi$, and $\langle E_{\nu_\mu}\rangle = 0.213 E_\pi$ respectively. The decay spectra from π^- are obtained by substituting particles accordingly.

---

[1] A. A. Penzias and R. W. Wilson, Astrophys. J. **142**, 419 (1965).

[2] K. Greisen, Phys. Rev. Lett. **16**, 748 (1966); G. T. Zatsepin and V. A. Kuz'min, Pis'ma Zh. Éksp. Teor. Fiz. **4**, 114 (1966) [JETP Lett. **4**, 78 (1966)].

[3] F. W. Stecker, Phys. Rev. Lett. **21**, 1016 (1968).

[4] J. L. Puget, F. W. Stecker, and J. H. Bredekamp, Astrophys. J. **205**, 638 (1976).

[5] *Astrophysical Aspects of the Most Energetic Cosmic Rays*, edited by M. Nagano and F. Takahara (World Scientific, Singapore, 1991).

[6] *Proceedings of the Tokyo Workshop on Techniques for the Study of Extremely High Energy Cosmic Rays*, Tokyo, Japan, 1993 (Institute for Cosmic Ray Research, University of Tokyo, 1993).

[7] M. A. Lawrence, R. J. O. Reid, and A. A. Watson, J. Phys. G **17**, 733 (1991); A. A. Watson, in *Astrophysical Aspects of the Most Energetic Cosmic Rays*, [5], p. 2.

[8] D. J. Bird *et al.*, Phys. Rev. Lett. **71**, 3401 (1993); Astrophys. J. **424**, 491 (1994).

[9] D. J. Bird *et al.*, Astrophys. J. **441**, 144 (1995).

[10] N. N. Efimov *et al.*, in Ref. [5], p. 20; T. A. Egorov in Ref. [6], p. 35.

[11] S. Yoshida *et al.*, Astropart. Phys. **3**, 105 (1995).

[12] N. Hayashida *et al.*, Phys. Rev. Lett. **73**, 3491 (1994).

[13] G. Sigl, S. Lee, D. N. Schramm, and P. Bhattacharjee, Science **270**, 1977 (1995).

[14] A. M. Hillas, Annu. Rev. Astron. Astrophys. **22**, 425 (1984).
[15] W. H. Sorrell, in Ref. [5], p. 329.
[16] P. Sommers, in Ref. [6], p. 23.
[17] J. W. Elbert and P. Sommers, Astrophys. J. **441**, 151 (1995).
[18] G. Sigl, D. N. Schramm, and P. Bhattacharjee, Astropart. Phys. **2**, 401 (1994).
[19] For a review see R. Blandford and D. Eichler, Phys. Rep. **154**, 1 (1987).
[20] T. K. Gaisser, *Cosmic Rays and Particle Physics* (Cambridge University Press, Cambridge, England, 1990).
[21] P. L. Biermann and P. A. Strittmatter, Astrophys. J. **322**, 643 (1987).
[22] C. T. Cesarsky, Nucl. Phys. B (Proc. Suppl.) **28B**, 51 (1992).
[23] C. A. Norman, D. B. Melrose, and A. Achterberg, Astrophys. J. **454**, 60 (1995).
[24] E. Waxman, Astrophys. J. Lett. **452**, L1 (1995).
[25] M. Vietri, Astrophys. J. **453**, 883 (1995).
[26] J. Miralda-Escude and E. Waxman, Astrophys. J. Lett. **462**, L59 (1996).
[27] C. T. Hill, Nucl. Phys. **B224**, 469 (1983).
[28] C. T. Hill, D. N. Schramm, and T. P. Walker, Phys. Rev. D **36**, 1007 (1987).
[29] P. Bhattacharjee, Phys. Rev. D **40**, 3968 (1989).
[30] P. Bhattacharjee, in Ref. [5], p. 382.
[31] P. Bhattacharjee and N. C. Rana, Phys. Lett. B **246**, 365 (1990).
[32] P. Bhattacharjee, C. T. Hill, and D. N. Schramm, Phys. Rev. Lett. **69**, 567 (1992).
[33] P. Bhattacharjee and G. Sigl, Phys. Rev. D **51**, 4079 (1995).
[34] G. Sigl, Space Sci. Rev. **75**, 375 (1996).
[35] *Proceedings of 24th International Cosmic Ray Conference*, Rome, Italy, 1995 (Istituto Nazionale Fisica Nucleare, Rome, 1995).
[36] T. Doi *et al.*, in Ref. [35], Vol. 2, p. 740.
[37] F. Halzen, R. A. Vazquez, T. Stanev, and H. P. Vankov, Astropart. Phys. **3**, 151 (1995).
[38] A. J. Gill and T. W. B. Kibble, Phys. Rev. D **50**, 3660 (1994).
[39] T. K. Gaisser (private communication).
[40] T. Weiler, Phys. Rev. Lett. **49**, 234 (1982); Astrophys. J. **285**, 495 (1984).
[41] S. Yoshida, Astropart. Phys. **2**, 187 (1994).
[42] G. Sigl and S. Lee, in Ref. [35], Vol. 3, p. 356.
[43] V. S. Berezinsky and S. I. Grigor'eva, Astron. Astrophys. **199**, 1 (1988).
[44] F. A. Aharonian, B. L. Kanevsky, and V. V. Vardanian, Astrophys. Space Sci. **167**, 93 (1990).
[45] J. P. Rachen and P. L. Biermann, Astron. Astrophys. **272**, 161 (1993).
[46] J. Geddes, T. C. Quinn, and R. M. Wald, Astrophys. J. **459**, 384 (1996).
[47] C. T. Hill and D. N. Schramm, Phys. Rev. D **31**, 564 (1985).
[48] S. Yoshida and M. Teshima, Prog. Theor. Phys. **89**, 833 (1993).
[49] F. A. Aharonian and J. W. Cronin, Phys. Rev. D **50**, 1892 (1994).
[50] J. Wdowczyk and A. W. Wolfendale, Astrophys. J. **349**, 35 (1990).
[51] F. A. Aharonian, P. Bhattacharjee, and D. N. Schramm, Phys. Rev. D **46**, 4188 (1992).
[52] R. J. Protheroe and P. A. Johnson, Astropart. Phys. **4**, 253 (1996).
[53] R. J. Protheroe and T. Stanev, Phys. Rev. Lett. **77**, 3708 (1996).
[54] S. Lee, A. V. Olinto, and G. Sigl, Astrophys. J. Lett. **455**, L21 (1995).
[55] S. Lee and G. Sigl, in Ref. [35], Vol. 2, p. 536.
[56] F. W. Stecker and O. C. De Jager, Astrophys. J. Lett. **415**, L71 (1993); O. C. De Jager, F. W. Stecker, and M. H. Salamon, Nature (London) **369**, 294 (1994).
[57] F. Halzen, R. J. Protheroe, T. Stanev, and H. P. Vankov, Phys. Rev. D **41**, 342 (1990).
[58] G. Sigl, K. Jedamzik, D. N. Schramm, and V. Berezinsky, Phys. Rev. D **52**, 6682 (1995).
[59] See, for example, *Proceedings of the International Workshop on Techniques to Study Cosmic Rays with Energies $\geq 10^{19}$ eV*, Paris, France, 1992, edited by M. A. Boratav, J. W. Cronin, and A. A. Watson [Nucl. Phys. B (Proc. Suppl.) **28B**, (1992)].
[60] S. W. Digel, S. D. Hunter, and R. Mukherjee, Astrophys. J. **441**, 270 (1995).
[61] C. E. Fichtel *et al.*, Astrophys. J. Lett. **217**, L9 (1977); D. J. Thompson and C. E. Fichtel, Astron. Astrophys. **109**, 352 (1982).
[62] J. L. Osborne, A. W. Wolfendale, and L. Zhang, J. Phys. G **20**, 1089 (1994).
[63] M. T. Ressell and M. S. Turner, Comments. Astrophys. **14**, 323 (1990).
[64] P. S. Coppi and F. A. Aharonian, Astrophys. J. Lett. **487**, L9 (1997).
[65] F. W. Stecker, O. C. De Jager, and M. H. Salamon, Astrophys. J. **390**, L49 (1992).
[66] D. MacMinn and J. R. Primack, Space Sci. Rev. **75**, 413 (1996).
[67] P. Mazzei, C. Xu, and G. De Zotti, Astron. Astrophys. **256**, 45 (1992).
[68] T. A. Clark, L. W. Brown, and J. K. Alexander, Nature (London) **228**, 847 (1970).
[69] M. S. Longair and R. Sunyaev, Usp. Fiz. Nauk **105**, 41 (1971) [Sov. Phys. Usp. **14**, 569 (1971)].
[70] J. S. Dunlop and J. A. Peacock, Mon. Not. R. Astron. Soc. **247**, 19 (1990).
[71] For a standard textbook discussion, see J. D. Jackson, *Classical Electrodynamics*, 2nd ed. (Wiley, New York, 1975).
[72] R. J. Protheroe and T. S. Stanev, Mon. Not. R. Astron. Soc. **264**, 191 (1993).
[73] A. A. Zdziarski, Astrophys. J. **335**, 786 (1988).
[74] P. S. Coppi and R. D. Blandford, Mon. Not. R. Astron. Soc. **245**, 453 (1990).
[75] R. W. Brown *et al.*, Phys. Rev. D **8**, 3083 (1973).
[76] A. Mastichiadis, Mon. Not. R. Astron. Soc. **253**, 235 (1991).
[77] E. Haug, Z. Naturforsch. A **30A**, 1099 (1975).
[78] A. Borsellino, Nuovo Cimento **4**, 112 (1947).
[79] K.-T. Kim *et al.*, Nature (London) **341**, 720 (1989); P. P. Kronberg, Rep. Prog. Phys. **57**, 325 (1994).
[80] R. J. Gould, Astrophys. J. **230**, 967 (1979).
[81] R. Svensson and A. A. Zdziarski, Astrophys. J. **349**, 415 (1990).
[82] A. A. Zdziarski and R. Svensson, Astrophys. J. **344**, 551 (1989).

[83] G. R. Blumenthal, Phys. Rev. D **1**, 1596 (1970).

[84] J. W. Motz, H. A. Olsen, and H. W. Koch, Rev. Mod. Phys. **41**, 581 (1969).

[85] M. J. Chodorowski, A. A. Zdziarski, and M. Sikora, Astrophys. J. **400**, 181 (1992).

[86] H. Genzel, P. Joos, and W. Pfeil, in *Landolt and Börnstein: Photoproduction of Elementary Particles* (Springer-Verlag, Heidelberg, 1973), Vol. 8, p. 1.

[87] K. C. Moffeit *et al.*, Phys. Rev. D **5**, 1603 (1972).

[88] Particle Data Group, R. M. Barnett *et al.*, Phys. Rev. D **54**, 1 (1996).

[89] C. T. Hill and D. N. Schramm, Phys. Lett. **131B**, 247 (1983).

[90] F. Halzen and A. D. Martin, *Quarks & Leptons: an Introductory Course in Modern Particle Physics* (Wiley, New York, 1984).

[91] See, e.g., E. W. Kolb and M. S. Turner, *The Early Universe* (Addison-Wesley, New York, 1990).

[92] A. Vilenkin, Phys. Rep. **121**, 263 (1985).

[93] A. Karle *et al.*, Phys. Lett. B **347**, 161 (1995).

[94] X. Chi, C. Dahanayake, J. Wdowczyk, and A. W. Wolfendale, Astropart. Phys. **1**, 129 (1993).

[95] X. Chi, C. Dahanayake, J. Wdowczyk, and A. W. Wolfendale, Astropart. Phys. **1**, 239 (1993).

[96] G. Sigl, S. Lee, and P. S. Coppi (unpublished).

[97] G. Sigl, S. Lee, D. N. Schramm, and P. Coppi, Phys. Lett. B **392**, 129 (1997).

[98] J. M. Quashnock, Astrophys. J. Lett. **461**, L69 (1996).